

RESEARCH ARTICLE

# The deubiquitinase USP6 affects memory and synaptic plasticity through modulating NMDA receptor stability

Fanwei Zeng<sup>1</sup>✉, Xuehai Ma<sup>1,2</sup>✉, Lin Zhu<sup>1</sup>✉, Qiang Xu<sup>1</sup>, Yuzhe Zeng<sup>1</sup>, Yue Gao<sup>1</sup>, Guilin Li<sup>1</sup>, Tiantian Guo<sup>1</sup>, Haibin Zhang<sup>1</sup>, Xiaoyan Tang<sup>3</sup>, Ziqiang Wang<sup>4</sup>, Zesen Ye<sup>1,5</sup>, Liangkai Zheng<sup>6</sup>, Hongfeng Zhang<sup>1</sup>, Qiuyang Zheng<sup>1</sup>, Kunping Li<sup>1</sup>, Jinfang Lu<sup>1</sup>, Xueting Qi<sup>1</sup>, Hong Luo<sup>1</sup>, Xian Zhang<sup>1</sup>, Zhanxiang Wang<sup>1,5</sup>, Yulin Zhou<sup>6</sup>, Yi Yao<sup>7</sup>, Rongqin Ke<sup>4</sup>, Ying Zhou<sup>8</sup>, Yan Liu<sup>3</sup>, Hao Sun<sup>1</sup>, Timothy Huang<sup>9</sup>, Zhicheng Shao<sup>1</sup>, Huaxi Xu<sup>9</sup>, Xin Wang<sup>1</sup>\*

**1** State Key Laboratory of Cellular Stress Biology, Fujian Provincial Key Laboratory of Neurodegenerative Disease and Aging Research, Institute of Neuroscience, School of Medicine, Xiamen University, Xiamen, China, **2** School of Life Sciences, Xinjiang Normal University, Urumqi, China, **3** Institute for Stem Cell and Neural Regeneration, School of Pharmacy, Nanjing Medical University, Nanjing, China, **4** School of Biomedical Sciences, Huaqiao University, Quanzhou, China, **5** Department of Neurosurgery, the First Affiliated Hospital of Xiamen University, Xiamen, China, **6** Women and Children's Hospital, School of Medicine, Xiamen University, Xiamen, China, **7** Department of Functional Neurosurgery, Xiamen Humanity Hospital, Xiamen, China, **8** Department of Translational Medicine, School of Medicine, Xiamen University, Xiamen, China, **9** Neuroscience Initiative, Sanford Burnham Prebys Medical Discovery Institute, La Jolla, California, United States of America

✉ These authors contributed equally to this work.

\* wangx@xmu.edu.cn



**OPEN ACCESS**

**Citation:** Zeng F, Ma X, Zhu L, Xu Q, Zeng Y, Gao Y, et al. (2019) The deubiquitinase USP6 affects memory and synaptic plasticity through modulating NMDA receptor stability. *PLoS Biol* 17 (12): e3000525. <https://doi.org/10.1371/journal.pbio.3000525>

**Academic Editor:** Jozsef Csicsvari, Institute of Science and Technology Austria, AUSTRIA

**Received:** April 23, 2019

**Accepted:** November 7, 2019

**Published:** December 16, 2019

**Copyright:** © 2019 Zeng et al. This is an open access article distributed under the terms of the [Creative Commons Attribution License](https://creativecommons.org/licenses/by/4.0/), which permits unrestricted use, distribution, and reproduction in any medium, provided the original author and source are credited.

**Data Availability Statement:** All relevant data are included in this publication and its associated Supporting Information files. Raw data on the Ubiquitin-modified proteome have been deposited in the iProX Consortium, a full member of the ProteomeXchange consortium, with the dataset identifier (Project ID) "IPX0001820000".

**Funding:** This work was partially supported by the National Natural Science Foundation of China (31871077, 81822014, 81571176 to XW; 81701349 to Hongfeng Z.; 81701130 to QZ; and

## Abstract

Ubiquitin-specific protease (USP) 6 is a hominoid deubiquitinating enzyme previously implicated in intellectual disability and autism spectrum disorder. Although these findings link USP6 to higher brain function, potential roles for USP6 in cognition have not been investigated. Here, we report that USP6 is highly expressed in induced human neurons and that neuron-specific expression of USP6 enhances learning and memory in a transgenic mouse model. Similarly, USP6 expression regulates *N*-methyl-D-aspartate-type glutamate receptor (NMDAR)-dependent long-term potentiation and long-term depression in USP6 transgenic mouse hippocampi. Proteomic characterization of transgenic USP6 mouse cortex reveals attenuated NMDAR ubiquitination, with concomitant elevation in NMDAR expression, stability, and cell surface distribution with USP6 overexpression. USP6 positively modulates GluN1 expression in transfected cells, and USP6 down-regulation impedes focal GluN1 distribution at postsynaptic densities and impairs synaptic function in neurons derived from human embryonic stem cells. Together, these results indicate that USP6 enhances NMDAR stability to promote synaptic function and cognition.

81471160 to HS), the National Key R&D Program of China (2016YFC1305900 to XW and HS), the Natural Science Foundation of Fujian Province of China (2017J06021 to XW), the Fundamental Research Funds for the Chinese Central Universities (20720150061 to XW and 20720180040 to ZS), Open Research Fund of State Key Laboratory of Cellular Stress Biology, Xiamen University (SKLCSB2019KF012 to QZ), and China Postdoctoral Science Foundation (2017M612130 to QZ). The funders had no role in study design, data collection and analysis, decision to publish, or preparation of the manuscript.

**Competing interests:** The authors have declared that no competing interests exist.

**Abbreviations:** AMPA,  $\alpha$ -amino-3-hydroxy-5-methyl-4-isoxazolepropionic acid; AMPAR, AMPA receptor; APP, amyloid precursor protein; ARHGAP11B, Rho GTPase activating protein 11B; BLBP, Brain lipid-binding protein; Calm1, Calmodulin 1; CAM, CamK2a; CamK2a, calcium/calmodulin dependent protein kinase II alpha; Cdh1, Cadherin 1; CNS, central nervous system; co-IP, coimmunoprecipitation; CTIP2, COUP-TF-interacting protein 2; CUX1, cut like homeobox 1; DUB, deubiquitinase; E, embryonic day; eEPSC, evoked excitatory postsynaptic current; ESC, embryonic stem cell; FDR, false discovery rate; FGF2, fibroblast growth factor 2; fEPSP, field excitatory postsynaptic potential; Glu, glutamate ionotropic receptor; GW, gestational week; HA, hemagglutinin; IgG, immunoglobulin G; IP, immunoprecipitation; KGG, anti-di-glycine remnant; LTD, long-term depression; LTP, long-term potentiation; MAP, Microtubule associated protein; mEPSC, miniature excitatory postsynaptic current; MWM, Morris water maze; N2aa, DMEM-F12 medium with N2-supplement and ascorbic acid; NEDD4, neural precursor cell expressed developmentally down-regulated protein 4; NMDA, *N*-methyl-D-aspartate; NMDAR, NMDA-type glutamate receptor; NOR, novel object recognition; NOTCH2NL, Notch 2 N-terminal like; NPC, neural progenitor cell; P, postnatal day; PP1, phosphatase 1; PSD, postsynaptic density; qRT-PCR, quantitative reverse transcription PCR; Rac1, Rac family small GTPase 1; Rho, Ras homolog; shRNA, short hairpin RNA; SRGAP2C, SLIT-ROBO Rho GTPase activating protein 2C; SRPX2, sushi repeat containing protein X-linked 2; Stx1b, syntaxin 1B; Syt, synaptotagmin; TBC, Tre-2/USP6, BUB2, and Cdc16; TBC1D3, TBC1 domain family member 3; TEM, transmission electron microscopy; TfR, transferrin receptor; TMEM14B, transmembrane protein 14B; Ub, ubiquitin; UBE3A, ubiquitin protein ligase E3A; UPS, ubiquitin-proteasome system;

## Introduction

Humans have evolved an advanced cognitive capacity over other mammalian species, featuring quantitatively enhanced functional abilities, such as learning and memory, as well as qualitatively new abilities such as speech. Human intelligence has been attributed to expanded regions in the cerebral cortex and enhanced complexity of neuronal connectivity in the human central nervous system (CNS). Genetic factors are thought to be fundamental to the evolution of the human brain. Several genes, including the hominoid-specific gene TBC1 domain family member 3 (*TBC1D3*) [1], the primate-specific gene Transmembrane protein 14B (*TMEM14B*) [2], and the human-specific genes Ras homolog (Rho) GTPase activating protein 11B 2 (*ARHGAP11B*) [3] and Notch 2 N-terminal like (*NOTCH2NL*) [4,5], have been found to be important for cortical development. In addition, synaptic wiring within the complex neural network contributes to advanced cognition and social function. The human neocortex contains approximately  $1.5 \times 10^{14}$  synaptic connections [6]. Pyramidal neurons in the human cortex form twice as many synapses as those in other primates, such as marmosets and macaques [7]. Several genes have been implicated in cognitive function through their involvement in synapse formation. SLIT-ROBO Rho GTPase activating protein 2C (*SRGAP2C*), a splice variant of *SRGAP2*, promotes synapse maturation by inhibiting the function of the *SRGAP2* gene [8]. Dysfunction of Sushi repeat containing protein X-linked 2 (*SRPX2*), which regulates synaptogenesis in cortical neurons, is associated with intellectual disability and language disorder [9,10].

Proper physiological function and the regulation of excitatory synapses in the CNS strongly correlate with cognitive ability [11]. Glutamate is the primary neurotransmitter in excitatory glutamatergic neurons in the mammalian brain [12]. Ionotropic  $\alpha$ -amino-3-hydroxy-5-methyl-4-isoxazolepropionic acid (AMPA) and *N*-methyl-D-aspartate (NMDA) glutamate receptors are the two major receptor types found within the postsynaptic density (PSD) of glutamatergic synapses, which transmit presynaptic signals to postsynaptic neurons [13]. NMDA-type glutamate receptor (NMDAR) stimulation triggers neuronal calcium influx through membrane-bound ion channels and activates intracellular calcium/calmodulin dependent protein kinase II alpha (CamK2a) or phosphatase 1 (PP1) signaling pathways. Stimulation of NMDAR-dependent calcium signaling pathways leads to the redistribution of AMPA receptors (AMPA receptors), resulting in synaptic changes associated with plasticity, such as long-term potentiation (LTP) or long-term depression (LTD), which form the physiological basis of learning and memory [14]. Modulation of GluN1 [15], GluN2B [16], and GluA1 [17] function through mutation or expression is associated with intellectual impairment. Distribution and regulation of NMDARs and AMPARs at PSDs is crucial to physiological synaptic function and cognition. Both NMDARs and AMPARs are degraded through the ubiquitin (Ub)-proteasome system (UPS) [18–22]. However, mechanisms underlying Ub targeting and the homeostatic maintenance of glutamate receptors in synaptic function remain largely unknown.

Ub-specific protease (USP) 6 is a hominoid-specific protein deubiquitinase (DUB) containing Tre-2/USP6, BUB2, and Cdc16 (TBC) and USP domains, and the *USP6* gene is found specifically in humans and orangutans [23]. USP6 TBC and USP domains are highly homologous to TBC1D3 and USP32 [23], respectively. Perturbation of USP6 expression through aberrant chromosomal translocation is associated with mental retardation [24] and Asperger syndrome [25]. In addition, a recent study revealed that TBC1D3 may play a crucial role in human intelligence by enhancing neural progenitor cell generation and cortical folding during development [1]. These findings suggest that the *USP6* gene may also be involved in the evolution of human intelligence.

Here, we generated a transgenic *USP6*-overexpression mouse model in which human USP6 is specifically expressed in excitatory neurons within the cerebral cortex and hippocampus.

USP, ubiquitin-specific protease; USV, ultrasonic vocalization; vGluT, Vesicular glutamate transporter; WT, wild-type.

USP6 transgenic mice exhibited enhanced learning and memory behavior in Morris water maze (MWM) and novel object recognition (NOR) tests. Moreover, transgenic USP6 expression increases synaptic function and NMDAR expression in USP6 transgenic mouse brains. Consistent with cognitive enhancement associated with USP6 gain of function, short hairpin RNA (shRNA)-mediated USP6 depletion in human embryonic stem cell (ESC)-derived neurons reduces NMDAR expression and function. We also found that USP6 binds to and deubiquitinates NMDARs, thereby enhancing NMDAR stability. In summary, we identified USP6 as a novel hominoid-specific regulator of NMDARs; USP6 enhances NMDAR stability through posttranslational homeostasis mechanisms, and its modulation can impact synaptic activity and memory formation.

## Results

### USP6 enhances learning and memory behavior in USP6 transgenic mice

Previous studies have shown that USP6 is expressed in multiple human tissues, and the highest expression is found in testes [23]. Using quantitative reverse transcription PCR (qRT-PCR) analysis, we found that USP6 expression was higher in the adult human cortex compared with fetal cortex (gestational week [GW] 22 to 27) (Fig 1A). To further characterize USP6 expression in different cell types in the CNS, we examined USP6 transcripts in H9 human ESCs, astrocytes, induced human excitatory neurons, and interneurons. USP6 mRNA levels are high in differentiated excitatory neurons and interneurons, whereas some expression was detectable in ESCs and astrocytes (Fig 1B).

To investigate the potential effects associated with *USP6* gain of function in mouse brain, we generated a transgenic mouse model expressing C-terminal hemagglutinin (HA)-tagged human USP6 under the regulation of the CamK2a promoter (CAM-USP6) (Fig 1C). Six independent founder lines were analyzed to detect USP6 protein expression, and two lines featuring elevated USP6 expression levels—i.e., USP6#1 (line 1) and USP6#2 (line 2)—were selected for breeding and analysis. Consistent with the CamK2a expression pattern previously characterized in mouse brain [26], we observed transgenic USP6 expression in the cortex and hippocampus, whereas its expression was undetectable in the cerebellum (Fig 1D). The body weight of CAM-USP6 mice (lines 1 and 2) was comparable to that of wild-type (WT) littermates (S1A Fig). Moreover, no significant difference in locomotor activity or anxiety was observed in open field tests, and CAM-USP6 transgenic animals did not differ from WT littermates in cumulative distance traveled (S1B Fig) or time spent in the central area (S1C Fig).

Given that *USP6* is a hominoid-specific gene and disruption of *USP6* gene expression by chromosomal translocation is associated with mental retardation [24], USP6 may play a role in higher cognitive functions in humans. To test this hypothesis, we firstly evaluated learning and memory in CAM-USP6 animals and their WT littermates using the NOR test and observed that CAM-USP6 transgenic animals spent more time in the zone containing novel objects and feature a higher discrimination index compared with WT controls (Fig 1E). In addition, we next examined the mice for spatial reference memory and reversal learning in the MWM task (Fig 1F) and found that CAM-USP6 transgenic animals required less time to reach the hidden platform during training in acquisition and reversal phase of MWM tests (Fig 1G). During the probe tests of both MWM and reversal learning, CAM-USP6 mice spent significantly more time in the target quadrant than WT mice (Fig 1H), indicating that USP6 overexpression enhances spatial memory and cognitive flexibility in CAM-USP6 mice. Because we observed comparable MWM trends in an additional USP6 transgenic line (line 2) (S2 Fig), the effects observed were unlikely to be due to gene disruption events from random insertion of the human USP6 cDNA.

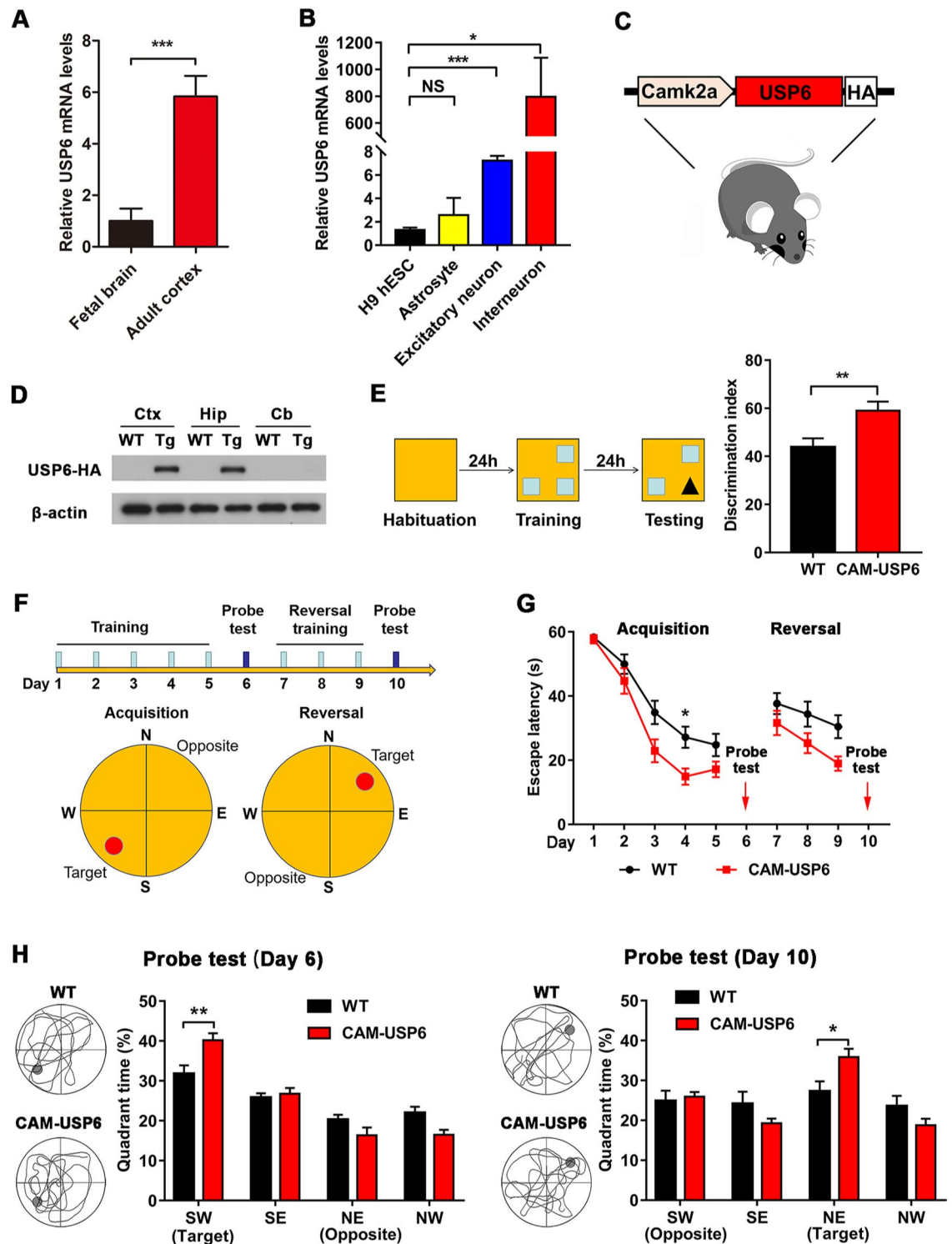


**Fig 1. Transgenic USP6 expression enhances learning and memory in mice.** (A) USP6 mRNA levels in the cortex of fetal and adult human brains were quantified by qRT-PCR. The data represent means  $\pm$  SEM,  $n = 5$ .  $***P < 0.001$  determined by Student  $t$  test. (B) USP6 mRNA levels in H9 hESCs, human astrocytes, induced human excitatory neurons, and interneurons were quantified by qRT-PCR. Data represent means  $\pm$  SEM,  $n = 15$ .  $**P < 0.01$ ,  $****P < 0.0001$  determined by nonparametric test (Kruskal-Wallis test) with Dunn's post hoc analysis. (C) Schematic diagram of the USP6 transgene under the regulation of a CamK2a promoter (CAM-USP6). (D) Immunoblot analysis of USP6-HA expression in the cortex, hippocampus, and cerebellum of CAM-USP6 mice. (E) Schematic diagram and results from NOR test analysis. Data represent means  $\pm$  SEM. WT:  $n = 16$  mice, CAM-USP6:  $n = 16$  mice.

\*\* $P < 0.01$  determined by Student  $t$  test. (F) MWM assessment of spatial memory and reversal learning. (G) MWM test results depicting escape latency as defined by the time taken to find a hidden platform. Data represent means  $\pm$  SEM. WT:  $n = 16$  mice, CAM-USP6:  $n = 16$  mice. \* $P < 0.05$  determined by repeated-measures ANOVA with Bonferroni's post hoc analysis. (H) MWM and reversal learning probe test results, acquisition phase: the target located in the SW quadrant; reversal learning: the target located in the NE quadrant. Data represent means  $\pm$  SEM. WT:  $n = 16$  mice, CAM-USP6:  $n = 16$  mice. \* $P < 0.05$ , \*\* $P < 0.01$  as determined by Student  $t$  test. The underlying data for this figure can be found in [S1 Data](#). CAM, CamK2a; CamK2a, calcium/calmodulin dependent protein kinase II alpha; Cb, cerebellum; Ctx, cortex; HA, hemagglutinin; hESC, human embryonic stem cell; Hip, hippocampus; MWM, Morris water maze; NE, northeast; NOR, novel object recognition; NS, not significant; NW, northwest; qRT-PCR, quantitative reverse transcription PCR; SE, southeast; SW, southwest; Tg, transgenic; USP, ubiquitin-specific protease; WT, wild-type.

<https://doi.org/10.1371/journal.pbio.3000525.g001>

## USP6 enhances social interaction and ultrasonic vocalization in vivo

Aberrant genetic disruption of the *USP6* locus is also associated with social behavior disorders, such as Asperger syndrome [25]. To determine whether transgenic *USP6* expression can affect social behavior in mice, we performed a three-chamber test (Fig 2A) and found that the CAM-USP6 mice spent more time approaching a “stranger” mouse compared with an empty cage during sociability test assays (Fig 2B). In social novelty tests, CAM-USP6 mice and littermate controls showed similar preference to a stranger mouse compared with a familiar animal (Fig 2C). We further characterized the communication behavior of CAM-USP6 pups through ultrasonic vocalization (USV) recordings. Pups separated from their mothers typically emit USV signatures that initiate a “search-and-retrieve” response in nearby mothers [9]. Isolation-induced pup USV behavior is an assay widely used to characterize mouse models of human diseases that involve deficits in language and social behavior [9,27,28]. CAM-USP6 pups vocalized more frequently than WT controls on postnatal day (P)7 (Fig 2D and 2E), indicating that transgenic *USP6* expression can enhance communication between pups and dams. Together, these results indicate that *USP6* up-regulation enhances spatial memory behavior and aspects of language and social interaction.

## USP6 expression does not affect cortical development in USP6 transgenic mice

Expression of the *USP6* paralog *TBC1D3* has been previously observed to induce cortical folding during brain development by increasing the production of neural progenitor cells. To investigate the potential role of *USP6* in embryonic neural development, we generated transgenic mice expressing *USP6* using a Nestin promoter (Nestin-USP6) (S3A Fig) and confirmed *USP6*-HA expression in embryonic day (E)18.5 Nestin-USP6 mouse brains (S3B Fig). Compared with WT controls, E16.5 Nestin-USP6 brains showed minimal to no difference in the number of radial glial cells stained by Brain lipid-binding protein (BLBP) and overall brain physiology/anatomy (S3C Fig). Further characterization of the postnatal Nestin-USP6 mouse cortex (P0 and P60) by Nissl staining showed a typical smooth surface with no apparent gyrus-like structures (S3D Fig). Moreover, the cerebral cortex from Nestin-USP6 mice was comparable to WT at P0 and P60 (S3D and S3E Fig). Visualization of Cut like homeobox 1 (*CUX1*) and COUP-TF-interacting protein 2 (*CTIP2*) markers, which specify layer II/III and layer V cortical neurons, respectively, demonstrated clear lamination in Nestin-USP6 mice; no differences in cortical *CUX1*<sup>+</sup>- or *CTIP2*<sup>+</sup>-labeled neurons were observed between Nestin-USP6 and WT mice on P60 (S3F Fig). We also observed no structural abnormalities in the cortex or hippocampus by Nissl staining in CAM-USP6 mice at 2 months (S4A Fig), and no differences in cortical thickness were observed (S4B Fig). Together, these results suggest that in contrast to previous results for *TBC1D3*, transgenic *USP6* expression did not significantly alter gross brain anatomy or cortical lamination/folding.

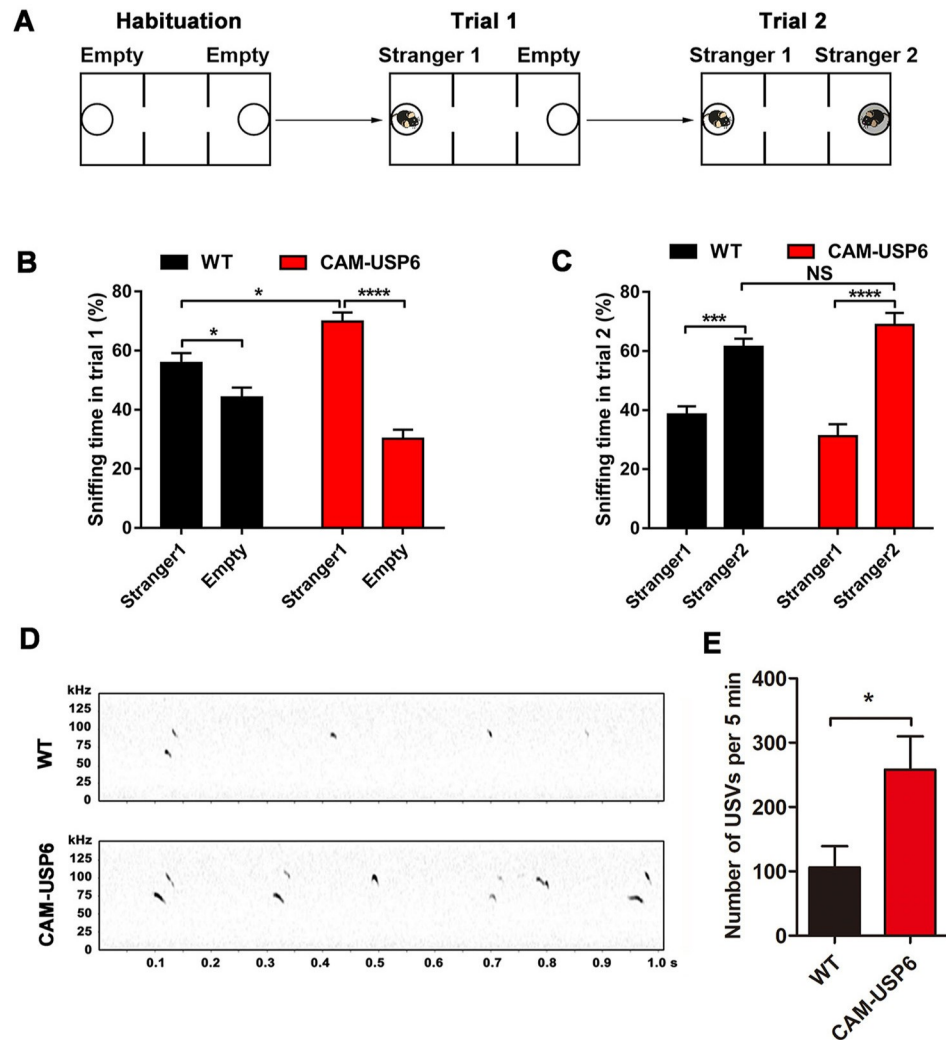


**Fig 2. USP6 enhances social behavior and USV vocalization in mice.** (A) Schematic diagram of social behavior using a three-chamber test. (B) Percent time spent sniffing the cage containing the mouse (Stranger 1) and empty cage (Empty) during the sociability test. Data represent means  $\pm$  SEM. WT:  $n = 16$  mice, CAM-USP6:  $n = 16$  mice. \* $P < 0.05$ , \*\*\*\* $P < 0.0001$  as determined by one-way ANOVA with Tukey's post hoc analysis. (C) Percent time spent sniffing the familiar (Stranger 1) and novel mice (Stranger 2) during the social novelty test. Data represent means  $\pm$  SEM. WT:  $n = 16$  mice, CAM-USP6:  $n = 16$  mice. \*\*\* $P < 0.001$ , \*\*\*\* $P < 0.0001$  as determined by one-way ANOVA with Tukey's post hoc analysis. (D) Representative spectrograph of USVs on P7 from CAM-USP6 and WT mice. (E) Number of USVs emitted within a 5-minute period by P7 CAM-USP6 pups. Data represent means  $\pm$  SEM. WT:  $n = 9$  mice, CAM-USP6:  $n = 9$  mice. \* $P < 0.05$  as determined by Student  $t$  test. The underlying data for this figure can be found in [S1 Data](#). CAM, CamK2a; NS, not significant; P, postnatal day; USP, ubiquitin-specific protease; USV, ultrasonic vocalization; WT, wild-type.

<https://doi.org/10.1371/journal.pbio.3000525.g002>

To determine whether USP6 expression affects synaptic density and morphology, we performed transmission electron microscopy (TEM) and Golgi staining and observed increased dendritic spine density in cortical layer II and V pyramidal neurons from CAM-USP6 mouse brain (S5A and S5B Fig). Although dendritic spine density of hippocampal CA1 pyramidal neurons in CAM-USP6 mice was found to be higher than in WT littermates, these trends were not found to be statistically significant (S5A and S5B Fig).

## CAM-USP6 mice display enhanced synaptic function

Thus far, we established that USP6 plays a role in memory/social behavior. To determine whether transgenic USP6 expression can enhance NMDAR-dependent synaptic function *in vivo*, we performed electrophysiological recordings using acute hippocampal slices from WT and CAM-USP6 mice. We observed comparable input–output responses (Fig 3A) and paired-pulse ratios (Fig 3B) between CAM-USP6 mice and WT littermate controls, suggesting that USP6 expression had minimal to no effect on basal synaptic transmission. To determine whether USP6 expression influences synaptic plasticity in CAM-USP6 mice, we examined NMDAR-dependent LTP and LTD responses in CAM-USP6 mice. We found that hippocampal CA1 LTP (100 Hz for 1 second) was enhanced (Fig 3C) and LTD (1 Hz for 900 seconds) was attenuated (Fig 3D) in CAM-USP6 compared with WT controls. As both AMPARs and NMDARs are involved in synaptic plasticity, we first examined miniature excitatory postsynaptic currents (mEPSCs) in hippocampal CA1 neurons from CAM-USP6 and WT mice and found that both mEPSC amplitude and frequency were unchanged between the two groups (S6 Fig). Given that AMPAR mEPSC recordings showed normal responses (S6 Fig), AMPAR function appears to be intact in both CAM-USP6 and WT mice. To characterize the potential differences in NMDAR function in the CAM-USP6 mice, we measured NMDA/AMPA ratios and evoked NMDA current (evoked NMDA receptor-mediated excitatory postsynaptic current [eEPSC]) in CAM-USP6 mice and WT controls; we observed increased NMDA/AMPA ratios and NMDA-eEPSC amplitudes in hippocampal CAM-USP6 CA1 neurons (Fig 3E and 3F). Together, these results indicate that USP6 expression enhances NMDAR-dependent synaptic function in CAM-USP6 mice.

## USP6 stabilizes NMDARs through its deubiquitinating activity

Thus far, mechanisms underlying USP6-mediated memory enhancement and social behavior appear to be independent of developmental events and changes in brain physiology. However, we observed USP6 distribution in synaptosome and PSD-enriched fractions using biochemical fractionation (S7 Fig), suggesting that USP6 may affect synaptic function through the deubiquitination of synaptic proteins. Therefore, we immunopurified trypsin-digested proteins extracted from mouse cortical tissue for peptides labeled with a di-Gly Ub-labeling signature and compared the relative abundance of these di-Gly peptides in cortical tissues from CAM-USP6 mice and WT controls (Fig 4A). Using this method, we identified 175 proteins (150 up-regulated and 25 down-regulated) that were differentially conjugated to Ub between CAM-USP6 and WT mouse brains (S1 Table).

Interestingly, we observed enrichment of di-Gly-labeled proteins involved in pathways related to synaptic function and plasticity, including LTP in WT versus CAM-USP6 transgenic mouse brain (Fig 4B and 4C). Differential Ub signatures were observed in the small Rho GTPase Rac family small GTPase 1 (Rac1), previously shown to be enriched in the hippocampus and contribute to LTP function [29], and synaptotagmin (Syt)1, which has been previously shown to work cooperatively with Syt7 in mediating LTP [30] (Fig 4D). Interestingly, we also observed differences in CAM-USP6 versus WT Ub signatures in postsynaptic components directly related to PSD function, including PSD95 and the NMDAR subunit GluN2B (Fig 4D). These results indicate that CAM-USP6 may drive changes in synaptic function to modulate/enhance memory, cognition, and social behavior.

To determine whether the expression of key targets identified in the Ub-associated proteome is altered in CAM-USP6 brain, we performed immunoblot analyses of proteins from CAM-USP6 and WT mouse brain. We observed up-regulation of GluN1, GluN2A, and GluN2B NMDAR subunits in CAM-USP6 mouse cortex and hippocampus, but little or no

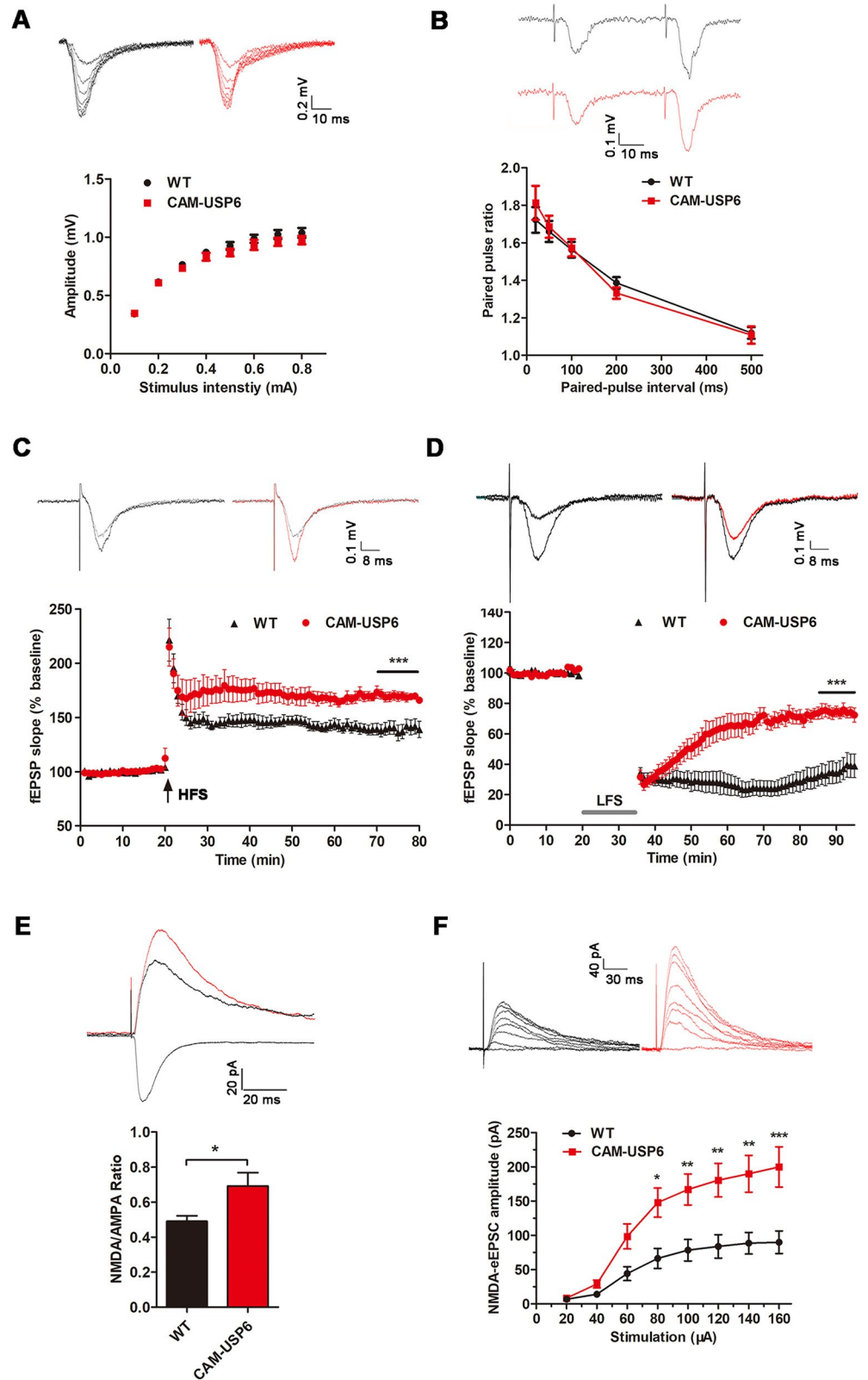


**Fig 3. USP6 enhances hippocampal LTP and attenuates LTD in an NMDAR-dependent manner.** (A) Input-output curves for basal synaptic transmission in hippocampal slices from WT ( $n = 3$  mice, 14 slices) and CAM-USP6 ( $n = 3$

mice, 8 slices) mice. Data represent means  $\pm$  SEM. (B) Paired-pulse ratio in WT ( $n = 3$  mice, 14 slices) and CAM-USP6 ( $n = 3$  mice, 10 slices) hippocampal CA1 neurons. Data represent means  $\pm$  SEM. Paired-pulse facilitation is calculated from the paired-pulse ratio (slope2/slope1). (C) NMDA-dependent LTP response. Slopes from fEPSPs before and after HFS (4 trains of 100-Hz stimulation for 1 second, 30-second interval) recorded from hippocampal slices. WT ( $n = 4$  mice, 4 slices), CAM-USP6 ( $n = 7$  mice, 10 slices). Data represent means  $\pm$  SEM. \* $P < 0.05$  as determined by a Student  $t$  test calculated from the last 10 minutes of recording. (D) NMDAR-dependent LTD response. Slopes of fEPSPs before and after LFS (1-Hz stimulation for 900 seconds) recorded from hippocampal slices are shown. WT ( $n = 4$  mice, 7 slices), CAM-USP6 ( $n = 4$  mice, 8 slices). Data represent means  $\pm$  SEM. \*\*\* $P < 0.001$  as determined by Student  $t$  test during the last 10 minutes of recording. (E) Sample traces of measurements and summary graphs of NMDA/AMPA receptor response ratios. WT ( $n = 3$  mice, 12 cells), CAM-USP6 ( $n = 3$  mice, 14 cells). Data represent means  $\pm$  SEM. \* $P < 0.05$  as determined by Student  $t$  test. (F) NMDA-eEPSC recordings in hippocampal CA1 neurons from 1-month-old WT ( $n = 3$  mice, 17 cells) and CAM-USP6 ( $n = 3$  mice, 26 cells) mice. Data represent means  $\pm$  SEM. \* $P < 0.05$ , \*\* $P < 0.01$ , \*\*\* $P < 0.001$  as determined by repeated-measures ANOVA with Bonferroni's post hoc analysis. The underlying data for this figure can be found in [S1 Data](#). AMPA,  $\alpha$ -amino-3-hydroxy-5-methyl-4-isoxazolepropionic acid; CAM, CamK2a; eEPSC, evoked excitatory postsynaptic current; fEPSP, field excitatory postsynaptic potential; HFS, high-frequency stimulation; LFS, low-frequency stimulation; LTD, long-term depression; LTP, long-term potentiation; NMDA, *N*-methyl-D-aspartate; NMDAR, NMDA-type glutamate receptor; USP, ubiquitin-specific protease; WT, wild-type.

<https://doi.org/10.1371/journal.pbio.3000525.g003>

difference was observed in GluA1 and GluA2 AMPAR levels ([Fig 5A and 5B](#)). We observed little or no change in glutamate receptor mRNA expression by qRT-PCR analysis of the CAM-USP6 mouse cortex, indicating that the differential NMDAR expression was due to modulation at the protein level as opposed to alterations in transcription ([S8 Fig](#)). To examine whether USP6 up-regulation can affect the distribution of NMDAR subunits to the cell surface, we subjected primary neurons from WT and CAM-USP6 mouse embryos to cell surface biotin-labeling assays. We observed significant up-regulation of cell surface GluN1, but no change was observed in the AMPAR subunit GluA1 or transferrin receptor (TfR), indicating that CAM-USP6 plays a potential role in enhancing cell surface NMDAR distribution ([Fig 5C](#)). Moreover, compared with WT controls, increased GluN1, GluN2A, and GluN2B levels were observed in both synaptosome and PSD-enriched fractions from CAM-USP6 mouse brains ([Fig 5D](#)). Given that these results suggest a role for USP6 in mediating physiological GluN1 homeostasis and cell surface distribution, we examined the effects of USP6 depletion in a human HEK293T cell line expressing GluN1. We found that shRNA-mediated USP6 depletion markedly down-regulated GluN1 protein expression and increased levels of ubiquitinated GluN1 ([S9 Fig](#) and [Fig 5E](#)). In contrast, GluN1 levels were not perturbed by shRNA-mediated TBC1D3 or USP32 depletion ([S10 Fig](#)), suggesting that USP6 mediates specific effects in targeting GluN1 for deubiquitination.

### USP6 interacts with NMDARs to attenuate UPS-mediated NMDAR turnover

After establishing a role for USP6 in modulating NMDAR ubiquitination and expression, we determined whether USP6 interacts with NMDAR subunits. Immunoprecipitation (IP) of USP6 from CAM-USP6 mouse brain lysates successfully demonstrates coprecipitation of USP6 with NMDAR subunits (GluN1 and GluN2B); no coimmunoprecipitation (co-IP) interaction was detected with AMPAR subunits (GluA1 and GluA2) and amyloid precursor protein (APP) ([Fig 6A](#)). We further characterized NMDAR binding to TBC or USP domain USP6 homologs (i.e., TBC1D3 and USP32); we found that both USP6 and TBC1D3 coimmunoprecipitated with GluN1/GluN2B, but USP32 failed to interact with NMDAR ([Fig 6B and 6C](#)). These results indicate that the N-terminal TBC domain is required for NMDAR interaction.

Subsequently, we compared ubiquitination of GluN1 in WT and CAM-USP6 mouse cortex; GluN1 IP using a GluN1 antibody and subsequent Ub immunoblot analysis for higher-molecular-weight poly-Ub conjugates demonstrated that USP6 expression reduced the levels of

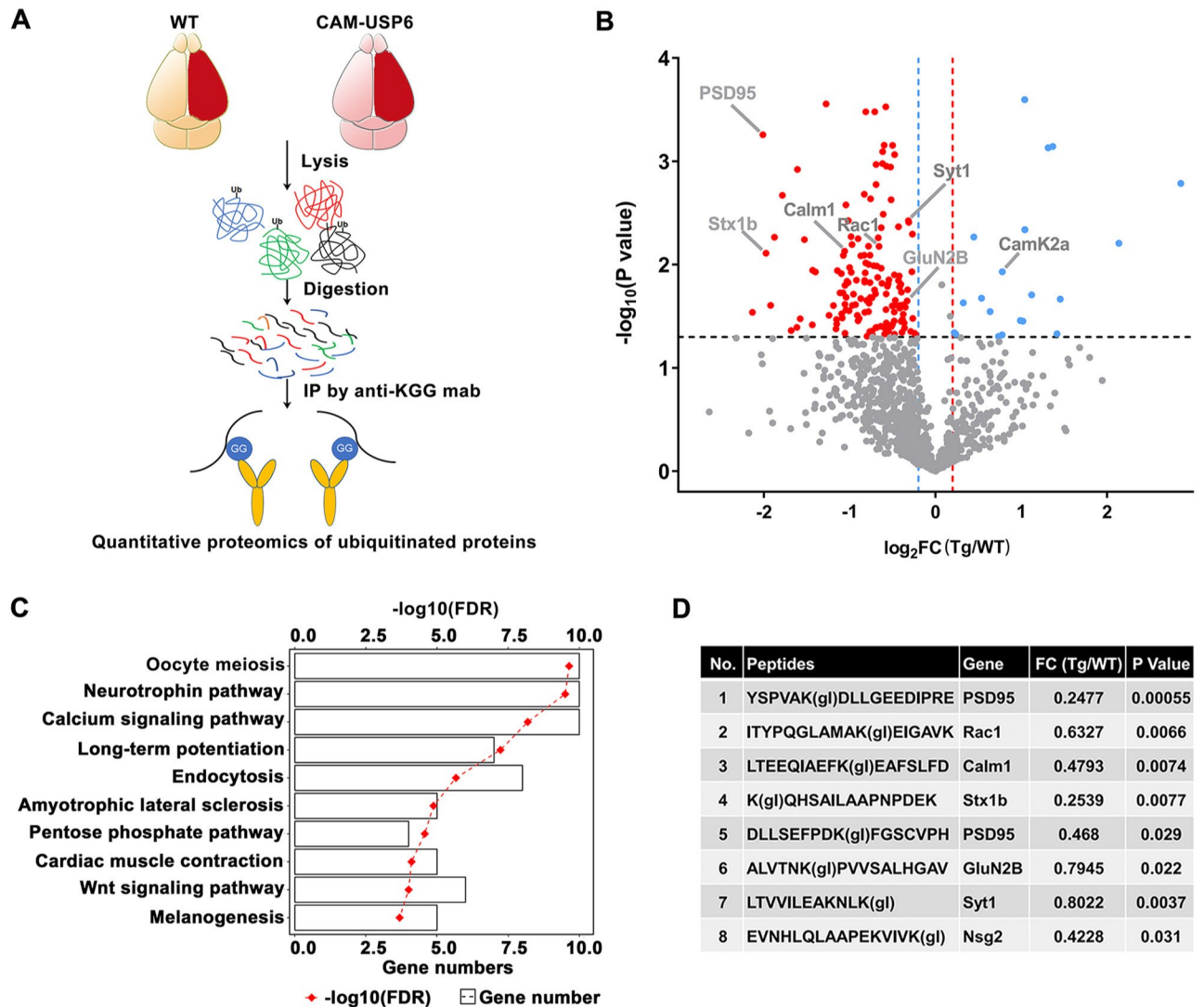


**Fig 4. Quantitative proteomic profiling of USP6-regulated proteins and signaling pathways.** (A) Schematic diagram depicting the quantitative proteomics pipeline used to identify differentially ubiquitinated proteins in CAM-USP6 Tg mouse brain. (B) Volcano plot indicating ubiquitinated protein species identified in CAM-USP6 compared with WT mouse brain cortex; colored plots represent significantly down-regulated (blue) and up-regulated (red) proteins.  $\log_{10} P$  value (*t* test, y-axis) and FC ( $\log_2$ FC, CAM-USP6 versus WT, x-axis) are shown. Significance cutoffs were set to  $P < 0.05$ ,  $FC > 1.2$ . (C) KEGG analysis of 175 differentially regulated proteins identified in CAM-USP6 versus WT mouse cortex. (D) Differentially ubiquitinated synaptic protein components identified in CAM-USP6 (compared with WT) mouse cortex. The underlying data for this figure can be found in [S1 Data](#). Calm1, Calmodulin 1; CAM, CamK2a; CamK2a, calcium/calmodulin dependent protein kinase II alpha; FC, fold change; FDR, false discovery rate; Glu, glutamate ionotropic receptor; IP, immunoprecipitation; KEGG, Kyoto encyclopedia of genes and genomes; KGG, anti-di-glycine remnant; PSD, postsynaptic density; Rac1, Rac family small GTPase 1; Stx1b, syntaxin 1B; Syt1, synaptotagmin 1; Tg, transgenic; USP, ubiquitin-specific protease; WT, wild-type.

<https://doi.org/10.1371/journal.pbio.3000525.g004>

polyubiquitinated GluN1 in vivo (Fig 7A). Furthermore, Ub IP and detection of GluN1 by immunoblotting demonstrated a reduction in GluN1 coprecipitation with Ub in CAM-USP6 brain (Fig 7B). We observed similar results in HEK293T cells; expression of GluN1-Myc or GluN2B-Myc together with USP6 markedly decreased levels of Ub-conjugated GluN1 and GluN2B (S11 Fig). Because this finding suggests that down-regulation of USP6 may enhance accumulation of Ub-conjugated GluN1, we indeed confirmed that shRNA-mediated USP6

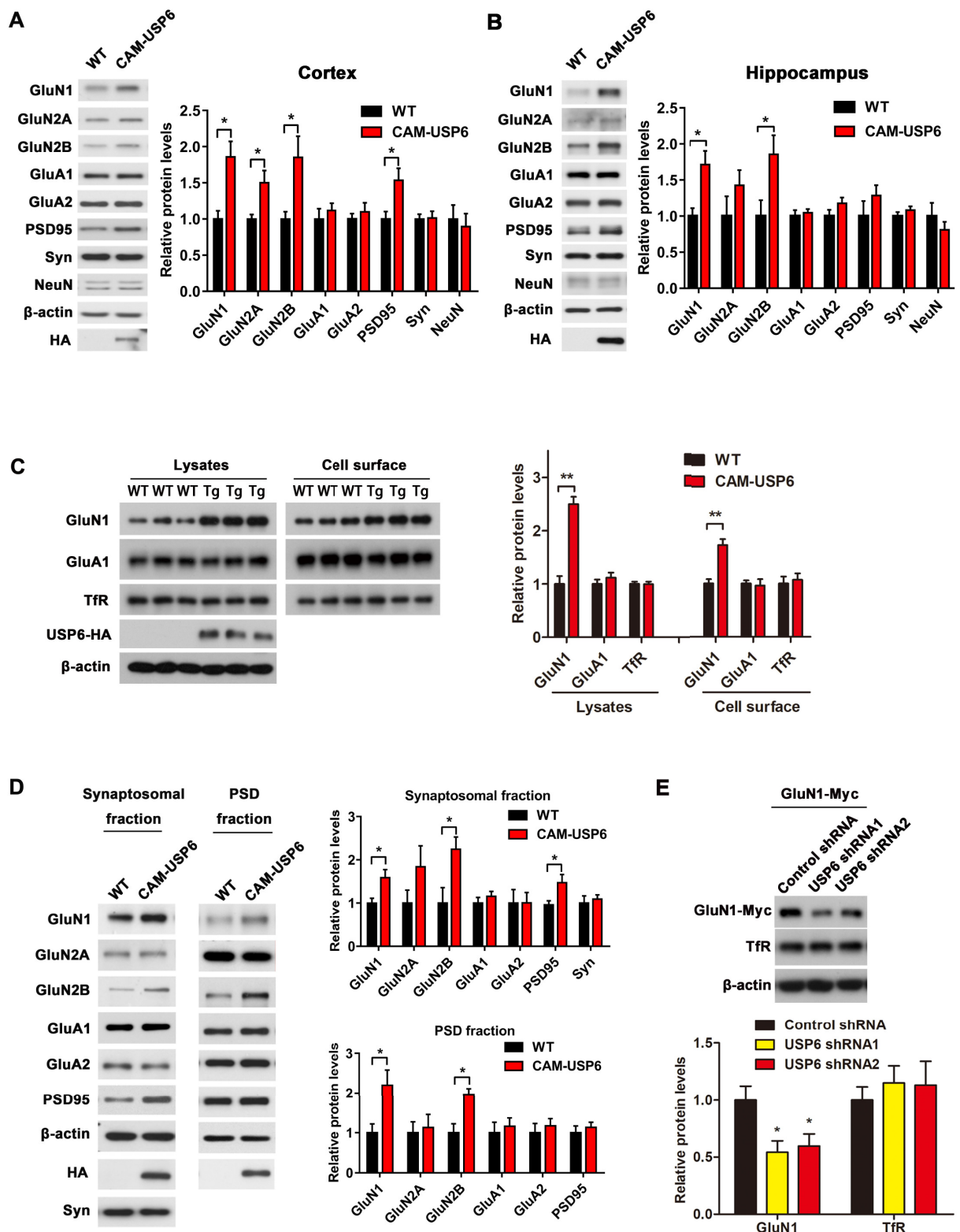


**Fig 5. Characterization of NMDA receptors as potential USP6 substrates.** (A and B) Immunoblot analysis of GluN1, GluN2A, GluN2B, GluA1, GluA2, Syn, PSD95, and NeuN in WT and CAM-USP6 mouse cortex (A) and hippocampus (B). Data represent means  $\pm$  SEM. Signal intensities from immunoblots were calculated and normalized to  $\beta$ -actin.  $n = 4$  mice.  $*P < 0.05$  as determined by Student  $t$  test. (C) Immunoblot analysis of cell

surface GluN1 levels in primary neurons from E18.5 CAM-USP6 mouse embryos; band densities were normalized to  $\beta$ -actin.  $n = 3$  mice,  $**P < 0.01$  as determined by Student  $t$  test. (D) Glutamate receptor subunit levels (GluN1, GluN2A, GluN2B, GluA1, GluA2) and PSD95 in synaptosomal and PSD fractions derived from WT and CAM-USP6 mouse cortex. Data represent means  $\pm$  SEM. Signal intensities from the immunoblots were normalized to  $\beta$ -actin.  $n = 4$  mice,  $*P < 0.05$  as determined by Student  $t$  test. (E) Immunoblot analysis of GluN1 levels in GluN1-expressing HEK293T cells transfected with USP6 shRNAs. The signal intensities of the immunoblots were normalized to  $\beta$ -actin.  $n = 3$ ,  $*P < 0.05$  as determined by one-way ANOVA with Tukey's post hoc analysis. The underlying data for this figure can be found in [S1 Data](#). CAM, CamK2a; Glu, glutamate ionotropic receptor; HA, hemagglutinin; NeuN, neuronal nuclei antigen; NMDA, *N*-methyl-D-aspartate; PSD, postsynaptic density; shRNA, short hairpin RNA; Syn, synaptophysin; TfR, transferrin receptor; Tg, transgenic; USP, ubiquitin-specific protease; WT, wild-type.

<https://doi.org/10.1371/journal.pbio.3000525.g005>

depletion in GluN1-Myc-transfected HEK293T resulted in accumulation of polyubiquitinated GluN1 following USP6 knockdown ([Fig 7C](#)).

To determine whether USP6 influences GluN1 turnover, we performed cycloheximide chase assays in HEK293T cells overexpressing GluN1; we found that GluN1 degradation was markedly accelerated by shRNA-mediated USP6 down-regulation ([Fig 7D](#)). Together, these results indicate that USP6 can interact with NMDAR subunits and promotes their stabilization by reducing NMDAR ubiquitination.

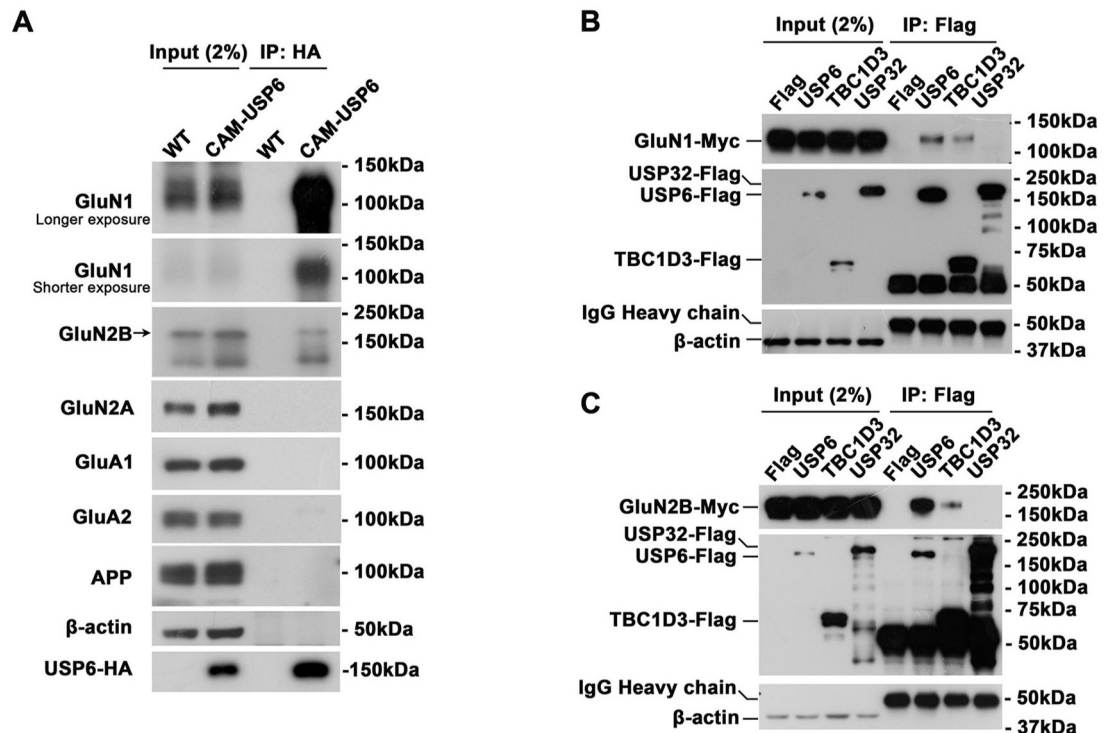


**Fig 6. USP6 interacts with NMDA receptors.** (A) Characterizing interactions between USP6-HA and glutamate receptor subunits by co-IP. WT and CAM-USP6 mouse brain lysates were precipitated with anti-HA magnetic beads, and precipitates were subsequently immunoblotted with antibodies to detect GluN1, GluN2B, GluA1, GluA2, APP, and  $\beta$ -actin. (B) co-IP interactions between exogenously expressed GluN1-Myc and Flag-tagged USP6, TBC1D3, or USP32. GluN1-Myc and USP6-Flag/TBC1D3-Flag/USP32-Flag were detected in lysates from cotransfected HEK293T cells; anti-Flag complexes were immunoprecipitated from lysates with an anti-Flag antibody and immunoblotted with a Myc antibody. (C) co-IP interactions detected between exogenously expressed GluN2B-Myc and USP6-Flag/TBC1D3-Flag/USP32-Flag. GluN1-Myc and USP6-Flag/TBC1D3-Flag/USP32-Flag were cotransfected into HEK293T cells, and complexes were immunoprecipitated from lysates with an anti-Flag antibody and immunoblotted with a Myc antibody. APP, amyloid precursor protein; CAM, CamK2a; co-IP, coimmunoprecipitation; Glu, glutamate ionotropic receptor; HA, hemagglutinin; IB, immunoblot; IgG, immunoglobulin G; IP, immunoprecipitation; NMDA, *N*-methyl-D-aspartate; TBC1D3, TBC1 domain family member 3; USP, ubiquitin-specific protease; WT, wild-type.

<https://doi.org/10.1371/journal.pbio.3000525.g006>

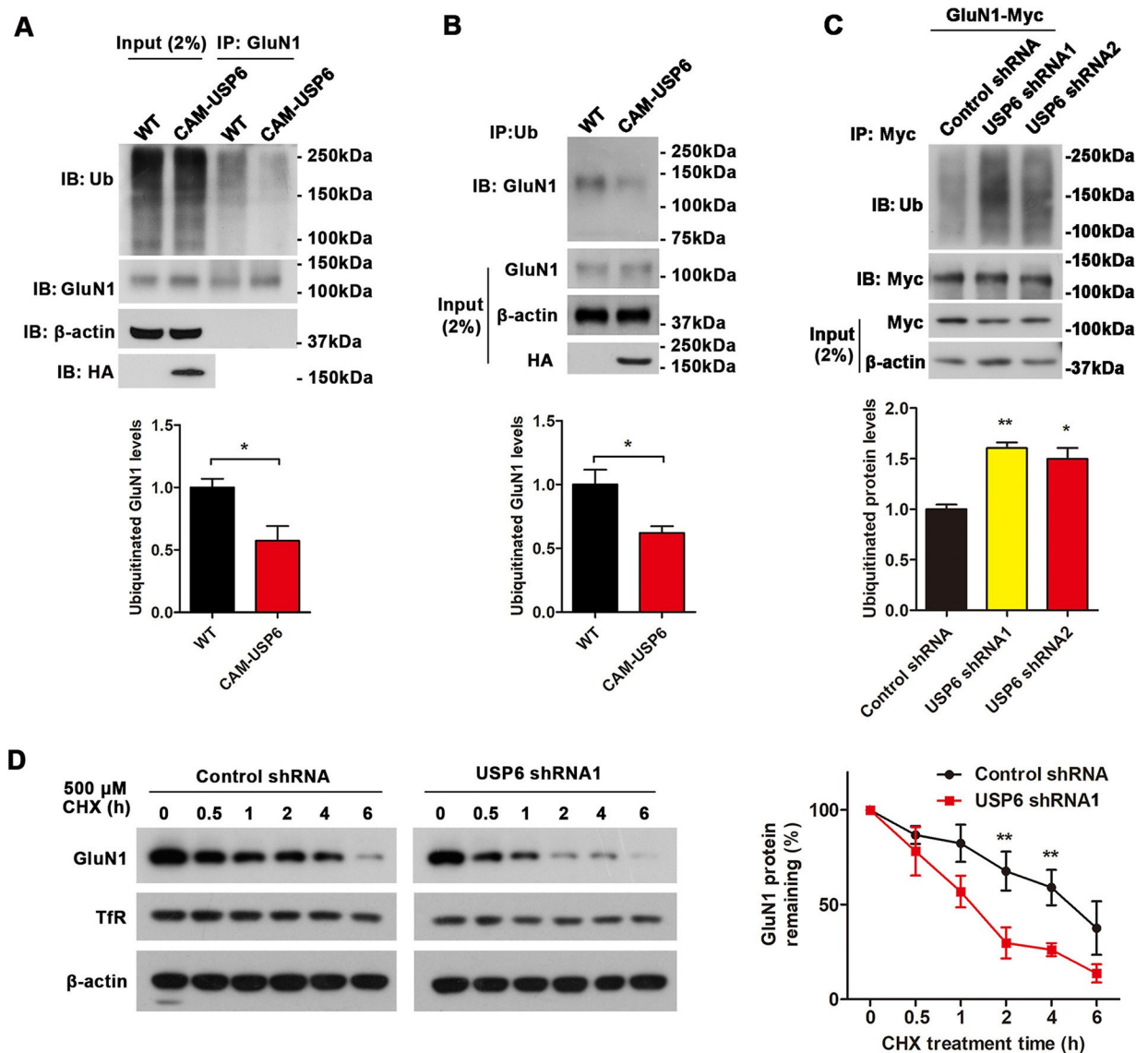


**Fig 7. USP6 attenuates NMDA receptor ubiquitination and enhances NMDA receptor stabilization.** (A) IB analysis to quantify polyubiquitinated GluN1 in WT and CAM-USP6 mouse cortex. Brain lysates were immunoprecipitated with an anti-GluN1 antibody and immunoblotted for Ub. IB band intensities were normalized to  $\beta$ -actin.  $n = 3$ . \* $P < 0.05$  as determined by Student  $t$  test. (B) IB analysis to quantify polyubiquitinated GluN1 in WT and CAM-USP6 mouse cortex. Brain lysates were immunoprecipitated with an anti-Ub antibody and immunoblotted for GluN1. IB band intensities were normalized to  $\beta$ -actin.  $n = 3$ . \* $P < 0.05$  as determined by Student  $t$  test. (C) IB analysis of polyubiquitinated GluN1 in HEK293T cells cotransfected with USP6-targeting shRNAs and GluN1-Myc. IB band intensities were normalized to  $\beta$ -actin.  $n = 3$ . \*\* $P < 0.01$  as determined by one-way ANOVA with Tukey's post hoc analysis. (D) Time course depicting GluN1 degradation with shRNA-mediated USP6 knockdown in GluN1-Myc transfected cells. Western blot analyses of GluN1-Myc and  $\beta$ -actin following CHX (500  $\mu$ M) treatment for the time indicated. GluN1 levels were normalized to  $\beta$ -actin and set to 100% at time 0. Data represent means  $\pm$  SEM.  $n = 3$ . \* $P < 0.05$  as determined by repeated-measures ANOVA with Bonferroni's post hoc analysis. The underlying data for this figure can be found in [S1 Data](#). CAM, CamK2a; CHX, cycloheximide; Glu, glutamate ionotropic receptor; IB, immunoblot; IP, immunoprecipitation; NMDA, N-methyl-D-aspartate; shRNA, short hairpin RNA; TfR, transferrin receptor; Ub, ubiquitin; USP, Ub-specific protease; WT, wild-type.

<https://doi.org/10.1371/journal.pbio.3000525.g007>

### USP6 depletion reduces NMDAR expression and function in ESC-derived human excitatory neurons

To investigate the effect of USP6 in a human neuronal model system, we differentiated human excitatory neurons from H9 ESCs (Fig 8A). To confirm successful differentiation of ESCs to

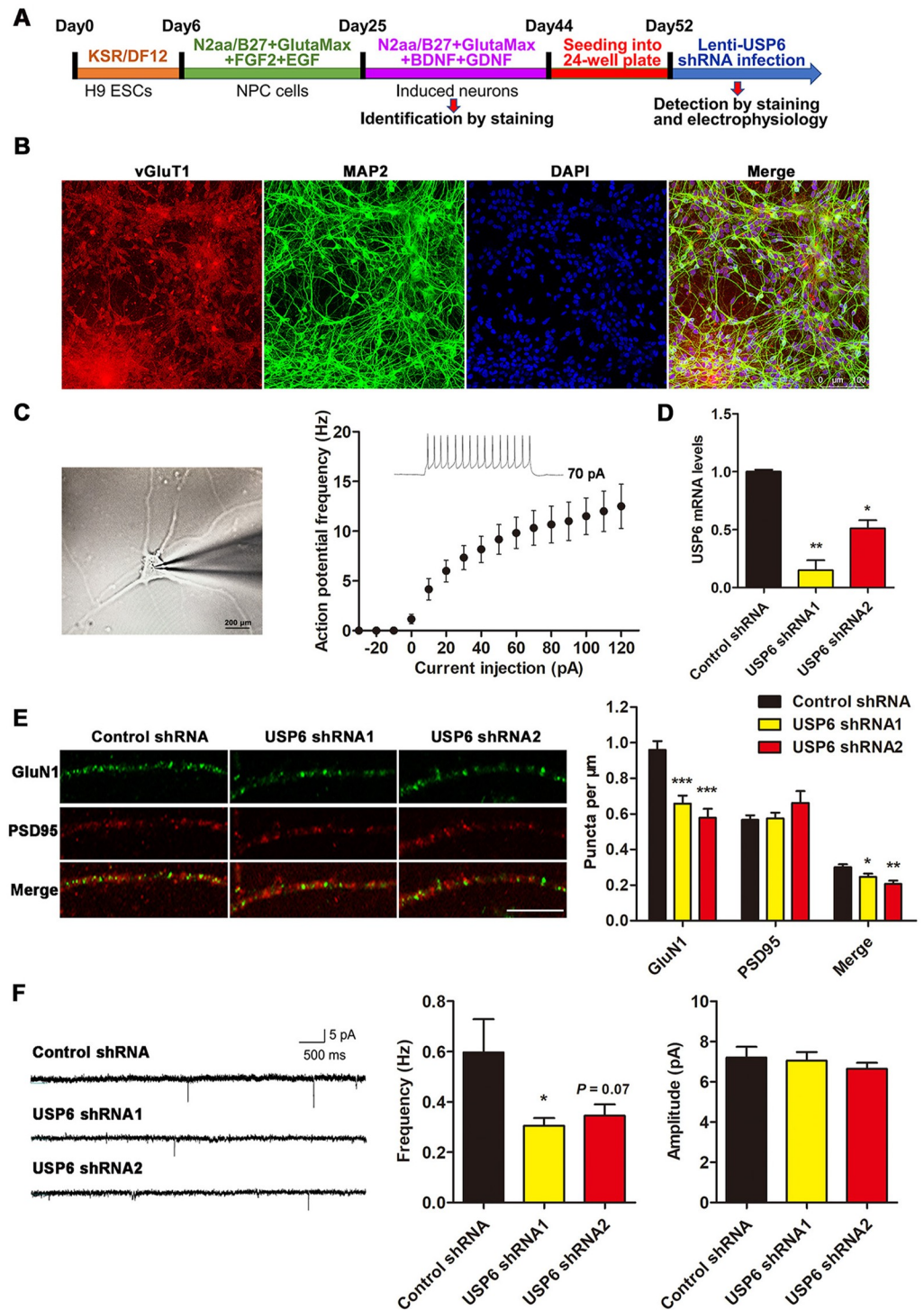


**Fig 8. USP6 depletion reduces GluN1 expression in ESC-derived human excitatory neurons.** (A) Schematic diagram depicting the differentiation timescale and experimental timeline in ESC-derived human excitatory neurons. (B) Immunostaining for vGluT1 and MAP2 at day 44 of differentiation. (C) Action potential at day 60 of differentiation in ESC-derived human excitatory neurons. (D) Knockdown efficiency of USP6 shRNAs in induced human excitatory neurons as quantified by qRT-PCR analysis. Data represent means  $\pm$  SEM.  $n = 3$ . \*\* $P < 0.01$ , \*\*\* $P < 0.001$  as determined by one-way ANOVA with Tukey's post hoc analysis. (E) Immunostaining for GluN1 and PSD95 in induced human excitatory neurons transduced with lentiviral USP6 shRNA. Quantification of GluN1 puncta: control shRNA ( $n = 43$  neurites from 36 neurons), USP6 shRNA1 ( $n = 36$  neurites from 19 neurons), and USP6 shRNA2 ( $n = 21$

neurites from 15 neurons); quantification of PSD95 puncta: control shRNA ( $n = 61$  neurites from 44 neurons), USP6 shRNA1 ( $n = 29$  neurites from 23 neurons), and USP6 shRNA2 ( $n = 21$  neurites from 15 neurons). The data represent means  $\pm$  SEM. \* $P < 0.05$ , \*\* $P < 0.01$ , \*\*\* $P < 0.001$  as determined by one-way ANOVA with Tukey's post hoc analysis. (F) Representative NMDA mEPSC recordings in induced human excitatory neurons infected with USP6 shRNA lentivirus. Data represent means  $\pm$  SEM.  $n = 3$ . \* $P < 0.05$  as determined by one-way ANOVA with Tukey's post hoc analysis. The underlying data for this figure can be found in [S1 Data](#). B27, B-27 serum-free supplement; BDNF, brain-derived neurotrophic factor; EGF, epidermal growth factor receptor; ESC, embryonic stem cell; FGF2, fibroblast growth factor 2; GDNF, glial cell-derived neurotrophic factor; Glu, glutamate ionotropic receptor; MAP2, microtubule-associated protein 2; mEPSC, miniature excitatory postsynaptic current; N2aa, DMEM-F12 medium with N2-supplement and ascorbic acid; NMDA, N-methyl-D-aspartate; NPC, neural progenitor cell; PSD, postsynaptic density; qRT-PCR, quantitative reverse transcription PCR; shRNA, short hairpin RNA; USP, ubiquitin-specific protease; vGluT1, vesicular glutamate transporter.

<https://doi.org/10.1371/journal.pbio.3000525.g008>

excitatory neurons, we performed Microtubule associated protein (MAP) 2 (dendritic marker) and Vesicular glutamate transporter (vGluT) 1 (excitatory neuron marker) costaining in mature differentiated neurons ([Fig 8B](#)). We also confirmed maturation by characterizing action potential response in differentiated neurons through patch-clamp recording in response to an increasing stimulus ([Fig 8C](#)).

To further determine whether USP6 loss of function negatively regulates GluN1 expression in ESC-derived human neurons, we used lentiviruses to transduce USP6-targeted shRNAs in differentiated neurons ([Fig 8D](#)). USP6 knockdown markedly diminished the formation of total dendritic GluN1 puncta and colocalized GluN1/PSD95 puncta ([Fig 8E](#)). In addition, shRNA-mediated down-regulation of USP6 diminished mEPSC frequency but had a minimal effect on mEPSCs in induced human excitatory neurons ([Fig 8F](#)). Together, these results indicate that USP6 down-regulation can reduce GluN1 clustering/distribution to PSD and impair mEPSC frequency in an ESC-derived human neuronal model.

## Discussion

*USP6* is a hominoid-specific gene that appeared during the evolution of the hominoid genome approximately 12–16 million years ago. The genomic *USP6* locus is prone to frequent chromosomal breakage and translocation events in which genomic rearrangement and consequent down-regulation of *USP6* expression likely leads to intellectual impairment and aberrations in social behavior, such as mental retardation and autism spectrum disorder [24,25]. Together, these findings suggest that *USP6* plays an important role in the evolution of human intelligence.

Protein homeostasis and regulatory mechanisms underlying protein synthesis and degradation are crucial for normal CNS function. Specific regulation of functional components involved in synaptic transmission is also subject to modulation by protein degradation mechanisms. Recent studies have highlighted the function of UPS in synaptic plasticity and various processes related to learning and memory [18,31,32]. However, how synaptic plasticity is coupled to the regulation of specific Ub proteases and the ubiquitination of specific proteins remains largely unclear. Although previous studies have indicated that numerous Ub ligases, including ubiquitin protein ligase E3A (UBE3A) [33–36], Neural precursor cell expressed developmentally down-regulated protein 4 (NEDD4) [37,38], and Cadherin 1 (Cdh1) [39,40], play a fundamental role in synaptic remodeling and function, opposing roles for DUB enzymes in regulating synaptic function have not been well characterized. Within the hominoid genome, *USP6* and *USP41* represent the sole hominoid-specific DUB enzyme species, suggesting that potential Ub-dependent regulatory mechanisms involving DUBs play a role in neurodegeneration and/or intelligence in hominoids. Our research reveals the pivotal role of *USP6* in regulating NMDAR ubiquitination and stability. Activation of NMDARs is required for

LTP and LTD at hippocampal CA1 synapses [41,42], implicating UPS-mediated synaptic remodeling in hominoid cognition. In addition to NMDARs, we identified other synaptic proteins as USP6 substrates, which can potentially contribute to enhancements in synaptic function. These substrates include the small Rho GTPase Rac1 and the synaptotagmin Syt1, which are components previously shown to be enriched in the hippocampus and important for LTP function [29,30]. In future studies, it will be of interest to determine whether mechanisms underlying synaptic plasticity are coupled to the activation or distribution of USP6 and its targets in learning and memory.

The UPS is a fundamental protein degradation system, and aberrant UPS function has been observed in several neurodegenerative diseases, such as Alzheimer disease, Parkinson disease, and Huntington disease [43]. Many neurodegenerative diseases feature the pathological appearance of intracellular Ub-positive inclusions that coincide with the proteostatic dysfunction of other aggregate-prone proteins in neurodegeneration [44]. Together, this suggests that UPS dysfunction in neurodegenerative disorders contributes to the accumulation of neurotoxic proteins that affect neurological decline and neurodegenerative onset. Based on our findings here, it will be interesting to determine the specific role of USP6-mediated protein turnover in neurodegenerative disease.

During human evolution, several primate- or human-specific genes have evolved, which may be fundamentally important to accommodate enhanced aspects of human cognition. Given that the *USP6* gene locus is located on a breakage-prone region within chromosome 17, *USP6* likely evolved through genomic translocation events resulting in the fusion of *TBC1D3* and *USP32*. Given that mutations in NMDAR subunits, such as GluN1 and GluN2B, have been previously linked to intellectual impairment [15,16], it appears reasonable that hominoid-derived factors may have evolved to enhance downstream effectors associated with synaptic function and cognition/memory. USP6 has evolved a unique capacity to enhance NMDAR function; although *TBC1D3* interacts with NMDARs, *TBC1D3* lacks a domain with deubiquitinating protease activity. Although *USP32* is a DUB, *USP32* requires a TBC domain to interact with NMDARs. Therefore, the combinatorial evolution of *USP6* may confer a unique function driving the enhancements in hominoid-specific synaptic function in the CNS.

Here, we also present a model system for studying hominoid-specific genes and characterizing their function in cognition; utilizing gain-of-function analysis in mouse models combined with shRNA-targeted gene depletion in human ESC-derived neurons, we established a systematic pipeline to determine how hominoid genes can affect cognition and intelligence. Furthermore, this system may enable subsequent studies investigating mutations in hominoid-specific genes manifesting disorders related to intelligence and social behavior. This system can also be used to recapitulate differential gene composition observed in various hominoid species, which may ultimately define how cognitive function evolved in humans.

In summary, we identified USP6 as a novel hominoid component that enhances NMDAR stability and function (Fig 9), in which USP6 plays a pivotal role in the evolution of intelligence. Given that NMDARs and their dysfunction have been implicated in human intelligence and cognition, enhancing USP6 function may be a potential option in future therapeutic studies.

## Materials and methods

### Ethics statement

All the protocols and procedures for the mice studies were approved by the School of Medicine, Xiamen University. The animal care and use protocol adhered to guidelines of Institutional Animal Care and Use Committee of Xiamen University. The human studies were

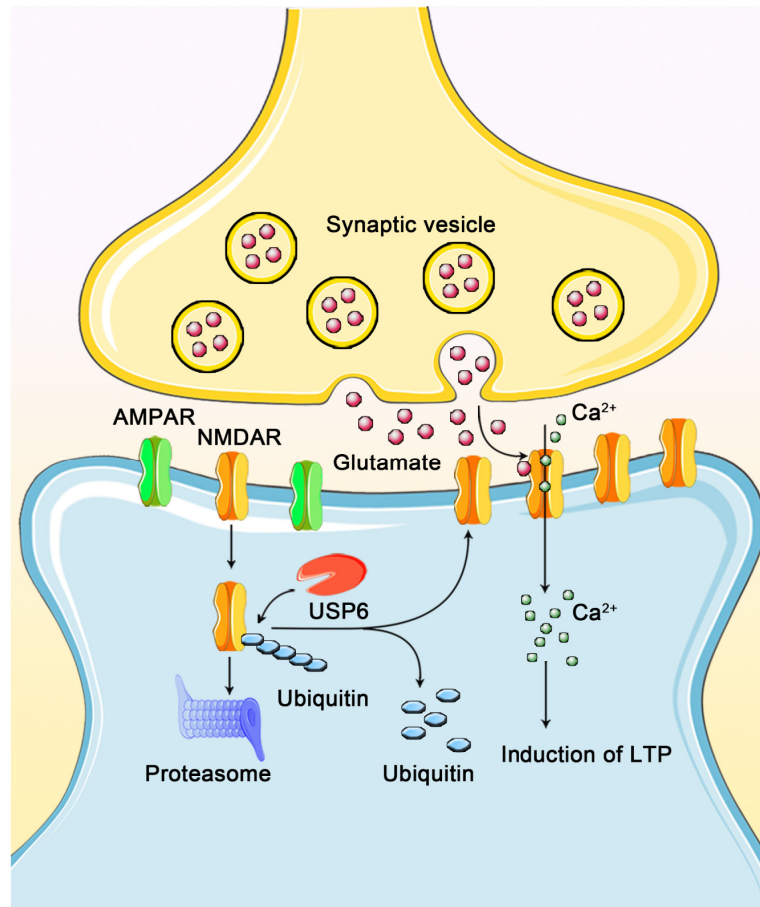


**Fig 9. A schematic model depicting USP6-dependent regulation of synaptic function.** The hominoid-specific gene *USP6* is required for maintaining synaptic function by stabilizing NMDARs. USP6 deubiquitinates NMDAR at the PSD, thereby facilitating NMDAR stabilization, resulting in increased NMDAR function and synaptic activity and enhanced cognition. AMPAR,  $\alpha$ -amino-3-hydroxy-5-methyl-4-isoxazolepropionic acid receptor; LTP, long-term potentiation; NMDAR, *N*-methyl-D-aspartate-type glutamate receptor; PSD, postsynaptic density; USP, ubiquitin-specific protease.

<https://doi.org/10.1371/journal.pbio.3000525.g009>

approved with informed consent by the ethical review board at the School of Medicine, Xiamen University (Project# XDYX2019011).

### Human brain collection

Human fetal brain tissue was collected and curated by the Women and Children’s Hospital, School of Medicine, Xiamen University (Table 1). Patients provided informed consent in accordance with the legal and institutional ethical guidelines defined by the hospital. Donors comprised pregnant women discontinuing their pregnancies due to congenital heart defects in the fetuses. All donors provided the fetal brains voluntarily and gave informed consent. Karyotype analysis confirmed that all fetal samples used had normal karyotypes. Adult brain tissue was collected from Xiamen Humanity Hospital following trauma surgery with informed patient consent according to the legal and institutional ethical requirements of the hospital (Table 1). All brain tissues were stored on dry ice and transported to the laboratory for subsequent examination and processing.

**Table 1. Tissue sample information from fetal and adult donors.**

Number	Group	Age	Gender	Tissue
1	Fetal brain	22 weeks	Male	Cortex
2	Fetal brain	26 weeks	Male	Cortex
3	Fetal brain	26 weeks	Male	Cortex
4	Fetal brain	27 weeks	Male	Cortex
5	Fetal brain	26 weeks	Male	Cortex
6	Adult brain	38 years	Male	Cortex
7	Adult brain	26 years	Male	Cortex
8	Adult brain	24 years	Male	Cortex
9	Adult brain	22 years	Male	Cortex
10	Adult brain	23 years	Male	Cortex

Human brain tissue used for qRT-PCR analysis in Fig 1A.

Abbreviation: qRT-PCR, quantitative reverse transcription PCR

<https://doi.org/10.1371/journal.pbio.3000525.t001>

## Animals

All experimental procedures and animal housing in this study were designed and conducted under the guidelines specified by the Institutional Animal Care and Use Committee of Xiamen University. CAM-USP6 and Nestin-USP6 transgenic mice were produced by Cyagen Biosciences. Briefly, the sequence of the CamK2a promoter (1,294 bp) or the Nestin promoter and the coding sequence of USP6 (NM\_004505.2) with a C-terminal HA tag were inserted into a PiggyBac vector to generate a pPB[Exp]-Promoter>hUSP6/HA construct. The plasmid was linearized and injected into the male pronucleus of C57BL/6 mice to generate heterozygous CamK2a or Nestin USP6 transgenic mice. All mice were housed and maintained at the institutional animal care facility under a 12:12-hour light/dark cycle.

## Antibodies

Antibodies used in this study were as follows: NeuN (mouse monoclonal antibody [mAb], Millipore, MAB337, 1:1,000), GluN2A (rabbit polyclonal antibody [pAb], Millipore, 556308, 1:1,000), GluN1 (mAb, BD, 556308, 1:1,000), GluN2B (mAb, BD, 610416, 1:1,000), PSD95 (mAb, Millipore, MAB1598, 1:2,000), synaptophysin (Sigma, SVP-38, 1:200), Myc (Invitrogen, 13-2500, 1:3,000), USP6 (pAb, Sigma, U2010, 1:1,000), Flag (mAb, Immunoway, YM1438, 1:3,000), HA (mAb, CST, 2999, 1:1,000), GluA1 (mAb, Millipore, 2508914, 1:1,000), GluA2 (pAb, Millipore, AB1768, 1:1,000),  $\beta$ -actin (mAb, xmbcss, bc001, 1:2,000), and Ub (mAb, Santa Cruz, 2508914, 1:1,000). The rabbit pAb 369 against the APP C terminus was described previously [45]. Secondary antibodies include goat anti-mouse IgG conjugate HRP (Thermo Fisher, 31430, 1:3,000), goat anti-rabbit IgG conjugate HRP (Thermo Fisher, 31460, 1:3,000), goat anti-mouse conjugate IgG Alexa Fluor 488 (Thermo Fisher, A-11001, 1:3,000), goat anti-rabbit conjugate IgG Alexa Fluor 488 (Thermo Fisher, A-11034, 1:3,000), goat anti-mouse IgG conjugate Alexa Fluor 594 (Thermo Fisher, A-11032, 1:3,000), and goat anti-rabbit conjugate IgG Alexa Fluor 594 (Thermo fisher, A-11037, 1:3,000). DNA was stained with DAPI (Vector-labs, H-1200).

## DNA constructs

cDNA fragments encoding USP6, TBC1D3, and USP32 were inserted into pCD513B-Flag, which was modified by inserting a Flag-tag into pCD513B-1 vector using EcoRI and BamHI

**Table 2. siRNA sequences.**

Target gene	siRNA sequences
Control siRNA	5'-UUCUCCGAACGUGUCACGUTT-3'
TBC1D3 siRNA1	5'-CCACAUCCUCCUGGCAUAUTT-3'
TBC1D3 siRNA2	5'-GCUGCCUCAUCCGGAUAUUTT-3'
TBC1D3 siRNA3	5'-GCGUUGAUGCCGAUAACAATT-3'
USP32 siRNA1	5'-CCUCCUUACAAGAGGCAAATT-3'
USP32 siRNA2	5'-GGGUUGAACUGAGAGACAUTT-3'
USP32 siRNA3	5'-CCGGAAGAAGAAGGACAAATT-3'

Abbreviations: siRNA, small interfering RNA; TBC, Tre-2/USP6, BUB2, and Cdc16; TBC1D3, TBC1 domain family member 3; USP, ubiquitin-specific protease

<https://doi.org/10.1371/journal.pbio.3000525.t002>

cloning sites. PCR fragments comprising GluN1, GluN2A, and GluN2B cDNA were cloned into pcDNA3.1 (Invitrogen).

shRNA targeting sequences for human USP6 (shRNA1: GGAGCGGAAGGACATACTT AT, shRNA2: TCATGCCCAGGATCGTGATAA) or scrambled shRNA (sequence: CCTAAG GTTAAGTCGCCCTCG) were inserted into a pLV-EGFP-Puro-U6 construct, and lentivirus was packaged by Cyagen Biosciences. siRNAs were purchased from Shanghai GenePharma Company, and sequence information is provided in [Table 2](#).

### Real-time PCR analysis

Tissue or cell samples were homogenized, and total RNA was isolated using TRIzol reagent (Invitrogen) according to the manufacturer's instructions. cDNA was synthesized using SuperScript III Reverse Transcriptase (TOYOBO) with random hexamers and OligdT primers. qRT-PCR was performed using a ROCHE 480 real-time LightCycler system and SYBR green reagent (ABI); primer sequence information is in [Table 3](#). At least three independent experiments were performed for all experiments described, and all results presented were calculated from CT values derived from the qRT-PCR reactions. All values were normalized to  $\beta$ -actin.

### Histology, immunofluorescence, and confocal imaging

Male mice were anesthetized with isoflurane followed by serial intracardial perfusion with PBS and 4% PFA [46]. Whole brains were rapidly dissected and postfixed in 4% PFA at 4°C overnight, dehydrated in PBS containing 30% sucrose at 4°C, and embedded and frozen in OCT at -80°C. Brain tissues were sectioned into 15- $\mu$ m slices using a Leica microtome. For histological analysis, frozen sections were stained with 1% cresyl violet (Beyotime) for Nissl staining. For immunofluorescence staining, brain sections were permeabilized using 0.1% Triton X-100 in PBS, blocked in 5% normal bovine serum in PBS, and incubated with primary antibodies at 4°C overnight. Fluorochrome-conjugated secondary antibodies were then used to detect primary antibody signals, and stained sections were imaged using a Leica SP8 confocal microscope.

### Neural differentiation from human ESCs

Human ESCs (H9, WiCell) were maintained on Matrigel (BD, 354480)-coated plates with Essential 8 (E8, GIBCO, A15171-01) medium. Neuronal differentiation from ESC lines was performed using a modified protocol [47]; H9 cells were trypsinized and maintained as floating spheres in low-adherence flasks in 15% KnockOut Serum (GIBCO, 10828028)-based medium (KSR/F12) (DMEM/F12, C11330500BT) with 100 nM LDN193189 (Stemolecule,

**Table 3. Primer sequences.**

Target gene	Primer sequences
Human USP6 F	5'-TGAGCCCGTTGGAATCAACA-3'
Human USP6 R	5'-ATCCACTTGCTCGTTCGTGT-3'
Human USP32 F	5'-AGATCAGGCTCCGACCCC-3'
Human USP32 R	5'-AGATCAGGCTCCGACCCC-3'
Human TBC1D3 F	5'-AGTGGTCTACAGCAGTTACACA-3'
Human TBC1D3 R	5'-GCTCGGTGCCCTTTTCGTA-3'
Human $\beta$ -actin F	5'-CAACCGCGAGAAGATGAC-3'
Human $\beta$ -actin R	5'-GTCCATCACGATGCCAGT-3'
Mouse GluA1 F	5'-AGGGATCGACATCCAGAGAG-3'
Mouse GluA1 R	5'-TGCACATTCCTGTCAAACC-3'
Mouse GluA2 F	5'-CAGTTTCGAGTCACCAATG-3'
Mouse GluA2 R	5'-ACCCAAAAATCGCATAGACG-3'
Mouse GluN1 F	5'-GGATACCAGATGTCCACCAGACTAAAG-3'
Mouse GluN1 R	5'-AACGCAGAAGCCATAACAGCAC-3'
Mouse GluN2A F	5'-CGGGTCTCATTTTCAGTCTTTACG-3'
Mouse GluN2A R	5'-GGTTGTCATCTGGCTCACAGTCAG-3'
Mouse GluN2B F	5'-GCGATTTGGTTACTCTGGGGTC-3'
Mouse GluN2B R	5'-GTCTCTGGAACCTTCTGTCACTCAGG-3'
Mouse $\beta$ -actin F	5'-GCCAACCGTGAAAAGATGAC-3'
Mouse $\beta$ -actin R	5'-GAGGCATACAGGGACAGCAC-3'

Abbreviations: F, forward; Glu, glutamate ionotropic receptor; R, reverse; TBC, Tre-2/USP6, BUB2, and Cdc16; TBC1D3, TBC1 domain family member 3; USP, ubiquitin-specific protease

<https://doi.org/10.1371/journal.pbio.3000525.t003>

04–0074) and 10  $\mu$ M SB-431542 (Tocris, 1614) for 5 days. In the following 24 days (6 to 24 days in vitro), the medium was changed to neurobasal medium (GIBCO, 21103–049) containing 2% B-27 (GIBCO, 17504–044), 1% GlutaMax (GIBCO, 35050–061), 20 ng/ml FGF-basic (PEPROTECH, AF-100-18B), 20 ng/ml EGF (PEPROTECH, AF-100-15), and 1% penicillin streptomycin (GIBCO, 15140–122). The medium was changed daily for the first 10 days and every other day for the subsequent 9 days. Differentiation medium was used at day 25: neurobasal medium, 2% B-27, 1% GlutaMax, 20ng/ml BDNF (PEPROTECH, AF-450-02), 20 ng/ml GDNF (PEPROTECH, AF-450-10), and 1% penicillin streptomycin (GIBCO, 15140–122). After 6 to 7 weeks of differentiation, cells were trypsinized with TrypLE Select (GIBCO, 12563–011) and seeded in 24-well or 6-well plates for 1–2 weeks, during which the medium was changed every 3 days. For the first 24 hours of seeding, cultures were supplemented with 1  $\mu$ M ROCK inhibitor Y-27632 (Batch, 1254). Expression of the excitatory neuronal markers vGluT1 (Synaptic systems, 135511) and MAP2 (Cell Signaling Technology, 4542S) were evaluated by immunofluorescence staining at day 44. ESC-derived neurons were transduced with lenti-USP6 shRNAs at day 52 to down-regulate USP6 expression. At 7 days postinfection, cells were processed for immunofluorescence and electrophysiological analysis. Quantification of GluN1 and PSD95 puncta was characterized in neurites of equivalent density and equidistant from the cell body.

### Interneuron differentiation from human ESCs

The interneuron induction was performed as previously described [48]. Human H9 ESCs were trypsinized and cultured as floating spheres in low adherent flasks in KSR medium

(DMEM, 15% knockout serum [GIBCO, 10828028]) replacement, 2 mM GlutaMax, and 10  $\mu$ M  $\beta$ -mercaptoethanol (Sigma, M3148) from day 0 to day 14. Rock inhibitor (Y-27632, 10  $\mu$ M, Tocris, 1254) was treated at day 1. For MGE-derived interneuron differentiation, from day 0 to day 7, LDN-193189 (100 nM Stemgent, 04-0074), SB431542 (10  $\mu$ M, Tocris, 1614), SAG (0.1  $\mu$ M, EMD Millipore, 566660), and IWP2 (5  $\mu$ M, EMD Millipore, 681671) were treated in the culture medium. From day 8 to day 14, cells were treated with LDN-193189 and SAG. From day 15 to day 21, the culture medium was changed with B27 medium (neurobasal with B27-supplement [2%, GIBCO, 17504-044], GlutaMax [1%, GIBCO, 35050-061], and ascorbic acid [200  $\mu$ M, Sigma]), and we added FGF8 (100 ng/ml, PEPROTECH, AF-100-25) and SAG. After 3 weeks, B27 medium was supplemented with 10 ng/ml GDNF (PEPROTECH, AF-450-02) and 10 ng/ml BDNF (PEPROTECH, AF-450-10) for neuronal maturation. After 6–7 weeks of differentiation, cells were trypsinized and seeded for analysis.

## TEM

TEM was used to detect synaptic ultrastructure as previously described [49]. Male mice were anesthetized with isoflurane followed by intracardial perfusion with PBS, followed by fixative containing 4% PFA and 2.5% glutaraldehyde. Tissue of frontal cortex and hippocampus were rapidly dissected, postfixed in fixative at 4°C overnight, and then postfixed by immersion in 1% osmium tetroxide at 4°C for 2 hours. The specimens were dehydrated in an ethanol gradient from 30% to 100% and embedded in Spurr's resin. After dehydration and embedment, serial ultrathin sections (70-nm in thickness) were prepared and stained with lead citrate and uranyl acetate, and TEM images were captured using a Hitachi HT-7800 transmission electron microscope. The number of synaptic connections was quantified using NIH ImageJ software by a person who was blinded to the animal genotype.

## Golgi staining

Golgi staining was performed in 2-month-old CAM-USP6 male transgenic mice using the FD Rapid Golgi Stain Kit (FD NeuroTechnologies) according to the manufacturer's instructions as previously described [50]. Dendritic spine density was imaged using a NIKON microscope in the CA1 region of the hippocampus and quantified using NIH ImageJ software [51]. Student *t* tests were used to determine statistical significance between WT and USP6 transgenic neurons.

## Ub-modified proteome

Ubiquitinated proteins were detected using an IP-MS/MS strategy as previously described [52,53]. Briefly, 2-month-old male WT and CAM-USP6 mouse cortices were collected and frozen in liquid nitrogen. Frozen samples were pooled and ground into a powder (1 g per sample) for total protein extraction using TCA-acetone. Proteins were resuspended in UA buffer (8 M urea, 150 mM Tris-HCl, pH 8.0), and lysates were sonicated, centrifuged, and filtered. Supernatants were collected and quantified by Bradford assay (Thermo Scientific Multiskan).

Protein (20 mg) was reduced using 1.25 mM dithiothreitol (DTT) for 30 minutes at 55°C, and resulting free cysteines were alkylated with 10 mM iodoacetamide for 15 minutes at room temperature in the dark. Approximately 20 mg of DTT and iodoacetamide-treated protein was digested overnight at 37°C with TPCK trypsin (Worthington) at an enzyme-to-substrate ratio of 1:50 after a 4-fold dilution in 20 mM 4-(2-hydroxyethyl)-1-piperazineethanesulfonic acid (HEPES) (pH 8.0). Trypsin digestion was stopped by the addition of trifluoroacetic acid to a final concentration of 1%. After precipitates were removed by centrifugation for 20 minutes at

10,000g, supernatants were desalted using Sep-Pak Classic C18 Cartridges (Waters) followed by lyophilization.

Lyophilized peptides were dissolved in immunoaffinity purification (IAP) buffer (50 mM MOPS–NaOH, pH 7.2, 10 mM Na<sub>2</sub>HPO<sub>4</sub>, and 50 mM NaCl) and centrifuged at 10,000g at 4°C for 10 minutes. For each sample, 250 µg of di-Gly-Lys antibody cross-linked on agarose beads (PTMScan Ub remnant motif K-ε-GG kit, Cell Signaling Technology) was used to immunopurify cleaved di-Gly Ub signatures, and di-Gly-Lys-containing peptides were enriched as previously described.

Fractions were individually injected for nanoLC-MS/MS analysis, and MS data were analyzed using MaxQuant software version 1.5.3.17 ([Max Planck Institute of Biochemistry in Martinsried, Germany](#)). Gene Ontology (GO) and KEGG pathway analysis was performed to characterize categorical gene function in the components identified.

### Preparation of synaptosome and PSD fractions

Hippocampal tissues from male mice were dissected and homogenized on ice in 10 volumes of cold sucrose buffer (0.32 M sucrose and 25 mM HEPES, pH 7.4) with protease inhibitors. Homogenates were centrifuged at 710g for 10 minutes at 4°C to isolate supernatant (S1) from large debris and nuclei. The S1 fraction was centrifuged at 10,000g for 15 minutes at 4°C. Supernatants were retained (S2; light membrane and cytosolic fraction), and pellets were washed twice with cold sucrose buffer and resuspended in cold HEPES-buffered saline (HBS) containing 25 mM HEPES and 150 mM NaCl (pH 7.4) to obtain synaptosome fractions. PSD-enriched fractions were prepared by solubilizing synaptosomes in 1% Triton HBS at 4°C for 30 minutes and, subsequently, centrifuging at 10,000g for 20 minutes. Pellets were resuspended in 3% sodium dodecyl sulfate (SDS) in HBS to yield PSD-enriched fractions [50,54].

### Immunoblot analysis

Brain tissues from male mice and samples comprising cultured cells were lysed on ice in RIPA lysis buffer (150 mM NaCl, 50 mM Tris-HCl [pH 8.0], 2 mM EDTA, 1% NP-40, 0.1% SDS, 0.5% sodium deoxycholate) or 0.5% TNEN lysis buffer (containing 20 mM Tris-HCl, pH 8.0, 100 mM NaCl, 1 mM EDTA, 0.5% NP-40) supplemented with protease inhibitors. Total protein concentration in brain homogenates or cell lysates was measured using a bicinchoninic acid assay (BCA) system (Thermo Fisher). Protein lysates were boiled in SDS loading buffer, and equivalent protein quantities (30–50 µg) were resolved by SDS-PAGE and western blotting, whereby blots were probed with primary antibodies and immunoreactive bands were quantified using NIH ImageJ software.

### co-IP assays

CAM-USP6 male mouse brain or transfected HEK293T cells were lysed in 0.5% TNEN lysis buffer supplemented with protease inhibitors. For all experiments, total protein concentration was determined by BCA assay (Thermo Fisher). Lysates were immunoprecipitated using anti-Myc, HA, or Flag antibodies in the presence of Protein G Dynabeads (Thermo Fisher), followed by immunoblot analysis.

### Field potential recordings

Female mice were anesthetized with isoflurane, and brains were rapidly removed and placed in ice-cold, high-sucrose cutting solution containing 120 mM sucrose, 64 mM NaCl, 26 mM NaHCO<sub>3</sub>, 10 mM glucose, 2.5 mM KCl, 1.25 mM NaH<sub>2</sub>PO<sub>4</sub>, 10 mM MgSO<sub>4</sub>, and 0.5 mM

CaCl<sub>2</sub>. Slices were sectioned on a Leica vibratome in high-sucrose cutting solution and immediately transferred to an incubation chamber with artificial cerebrospinal fluid (ACSF) containing 120 mM NaCl, 26 mM NaHCO<sub>3</sub>, 10 mM glucose, 3.5 mM KCl, 1.25 mM NaH<sub>2</sub>PO<sub>4</sub>, 1.3 mM MgSO<sub>4</sub>, and 2.5 mM CaCl<sub>2</sub>. Slices were allowed to recover at 32°C for 1 hour before equilibration at room temperature for 1 hour. During recordings, slices were placed in a recording chamber perfused with ACSF and continuously aerated with 95% O<sub>2</sub>/5% CO<sub>2</sub>.

For LTP field recordings, the Shaffer collateral was stimulated with a concentric bipolar electrode placed in the CA3 stratum radiatum. Field potentials in the CA1 stratum radiatum were recorded using a micropipette filled with ACSF. Baseline responses were obtained every 20 seconds with a stimulation intensity that yielded a 30%–40% maximal amplitude (mV) response. LTP was induced by four trains of high-frequency stimulation (100 Hz, 1 second) separated by 30-second intervals. For LTD field recordings, concentric bipolar and patch electrodes were placed as described in the LTP protocol above. Baseline responses were obtained every 20 seconds with a stimulation intensity that yielded a 50%–60% maximal amplitude (mV) response. LTD stimulation was induced at a frequency of 1 Hz for 900 seconds. For input–output recordings, electrical stimulation in the CA3 stratum radiatum was applied sequentially in a gradient ranging from 0 to 0.8 mA in 0.1-mA steps. For paired-pulse ratio recordings, two pulses with stimulation intensities that yielded a 40% maximal amplitude (mV) response spaced at determined time intervals (20, 50, 100, 200, and 500 milliseconds) were administered.

### Whole-cell patch-clamp recordings

Acute hippocampal slices from female mice were processed and maintained as described above. To obtain NMDAR- to AMPAR-EPSC ratios, a concentric bipolar electrode was placed in the stratum radiatum to evoke EPSCs in CA1 pyramidal cells. CA1 pyramidal cells were affixed to patch electrodes containing 140 mM CsCH<sub>3</sub>SO<sub>3</sub>, 2 mM MgCl<sub>2</sub>·6H<sub>2</sub>O, 5 mM TEA-Cl, 10 mM HEPES, 1 mM EGTA, 2.5 mM Mg-ATP, and 0.3 mM Na-GTP (pH 7.2–7.4). AMPAR-EPSC was first recorded at –70 mV in ACSF (containing 100 μM picrotoxin [PTX]). Mixed AMPAR-EPSC and NMDAR-EPSC outputs were then recorded at +40 mV using the same stimulation pulse (100 μA). Peak NMDAR-EPSC was calculated at 50 milliseconds from the initial mixed EPSC output.

NMDAR-mediated eEPSCs (NMDA-eEPSCs) were recorded in the presence of 20 μM 6-cyano-7-nitroquinoxaline-2,3-dione (CNQX) and 100 μM PTX. An additional 5 mM QX314 was added to the internal solution to block voltage-dependent sodium channels at the intracellular interface. NMDAR-eEPSC was recorded at +40 mV. A concentric bipolar electrode was placed 200–250 μm from the neuron recorded. Synaptic currents were elicited by increasing stimulation intensities (ranging from 0–160 μA in 20-μA steps) administered at a frequency of 0.05 Hz. AMPAR-mediated mEPSCs (AMPA-mEPSCs) were recorded in the presence of 1 μM tetrodotoxin (TTX), 50 μM AP5, and 100 μM PTX at a holding potential of –70 mV.

Action potentials in induced human excitatory neurons were recorded in current-clamp mode, in which recording pipettes were filled with intracellular solution containing (in mM): 122 K-gluconate, 5 NaCl, 0.3 CaCl<sub>2</sub>, 2 MgCl<sub>2</sub>, 1 egtazic acid (EGTA), 10 HEPES, 5 Na<sub>2</sub>-ATP, and 0.4 Na<sub>3</sub>-GTP; pH was adjusted to 7.2–7.3 with KOH, and the osmolarity was adjusted to 280 mOsm/kg with sucrose. Action potentials were generated by direct intracellular current injections (500 milliseconds) of increasing magnitude (in 10-pA steps) from –30 pA to 120 pA. In current-clamp mode, NMDAR-mediated mEPSCs (NMDA-mEPSCs) were recorded in the presence of 1 μM TTX, 20 μM CNQX, and 100 μM PTX with a Cs-based internal solution at a holding potential of –70 mV.

### Open field test

In open field tests, the behavior of each mouse was characterized in an open field box (60 × 60 cm, height 60 cm), and total distance traveled was monitored to assess motor behavior. Percentage of the time spent in the center zone was recorded to determine anxiety-like behavior. To exclude estrogenic effects, only male mice were used in behavior tests.

### MWM and reversal learning

MWM were performed as previously described [55,56]. The tests were conducted in a light-blue circular pool (diameter 1.2 m, height 0.5 m) filled with opaque water maintained at 22°C. Four spatial markers comprising different shapes visible to the animals were affixed on the walls of the pool. A round fixed platform (diameter 10 cm) was submerged approximately 1–2 cm below the water level. On training days, the mouse was forced to swim in the water and allowed to search for 60 seconds to find the hidden platform, where the mouse remained for 10 seconds. For cases in which the mouse was unable to find the platform, the mouse was guided to the hidden platform and allowed to remain on the platform for 10 seconds. Each mouse was trained for 6 days with four trials per day from four different quadrants used to enter the pool. Mouse behavior was monitored and analyzed using Smart 3.0 software (Pan-lab), and escape latency was scored for each trial. On the last day, a probe test was performed without the platform, and mice were allowed to swim for 60 seconds; the probe test was performed with two trials; time spent in each quadrant and the target platform quadrant were subsequently analyzed [55]. Reversal learning was performed based on the MWM, with the following adjustments: each mouse was trained for 6 days with two trials per day from two different quadrants used to enter the pool, and the probe test was performed with one trial to reduce swimming intensity. After the probe test, the platform was moved to the opposite quadrant, and each mouse was trained for 3 days with 2 trials per day from two different quadrants used to enter the pool. On the last day, a second probe test was performed without the platform, and mice were allowed to swim for 60 seconds; time spent in each quadrant and the target platform quadrant were subsequently analyzed [56].

### NOR

NOR was used to detect learning and memory according to a previous method [57]. At 24 hours before testing, each mouse was habituated for 5 minutes in a chamber (40 × 40 × 40 cm). During testing, the mouse was exposed to a set of three identical objects in the chamber for 10 minutes. The mouse was then removed from the chamber for 2 minutes while the chamber was cleaned with 70% ethanol and one of the objects was replaced with a novel object. The mouse was then returned to the chamber, and the interaction time with the two familiar or novel objects was recorded. Total interaction time was determined as the sum of interaction times (familiar 1 + familiar 2 + novel object). The discrimination index (%) was defined as time spent exploring the novel object/total interaction time × 100. An interaction was defined as active investigation of the object while the mouse was oriented toward and within 1 cm of the object. Mice with a total interaction time of less than 3 seconds were excluded from analysis.

### Three-chamber test

Social communication behavior was performed using a three-chamber test as previously described [58]. The apparatus consisted of a plexiglass chamber comprising three equally sized compartments, where the mouse was allowed to explore three chambers using two sliding

doors. Smart 3.0 software (Panlab) was used to record and analyze mouse behavior. Two wire cages were placed in the left and right chamber, respectively. The test consisted of three phases: (1) During habituation, the test mouse was placed in the center chamber and allowed to freely explore chambers for 5 minutes. (2) Sociability tests were performed in which an unfamiliar mouse (stranger 1) was introduced into a wire cage in one side of the chamber as the stimulus mouse. Location of stranger 1 in the left- or right-side chamber was evenly balanced across subjects. The test mouse was allowed to freely explore the chambers for 10 minutes. The time sniffing the wire cage with stranger 1 or the empty cage was recorded. (3) In the social novelty test phase, a new unfamiliar mouse (stranger 2) was placed into the empty cage, and then the test mouse was allowed to freely explore each chamber for 10 minutes. The time sniffing the wire cage with stranger 1 or stranger 2 was recorded.

### USV recording

Isolation-induced USV in infant pups was assessed as previously described [58] using hardware and software provided by Avisoft Bioacoustics. At 10 minutes prior to initiating the experiment, the dam was separated from its litter to create a stable pretest baseline. P7 pups were isolated from their housing cages and individually placed in a recording box situated in an anechoic chamber [8,9]. An ultrasonic microphone was positioned approximately 5 cm above the pup and set to record vocalizations of 50–100 kHz with a 40-dB cutoff over a 5-minute recording period.

### Statistical analysis

Statistical analyses were performed with GraphPad Prism. The data distribution was assessed by a Kolmogorov-Smirnov nonparametric test of equality. Differences between two means were assessed by Student *t* test. Differences among multiple means were assessed, as indicated, by one-way, two-way, or repeated-measures ANOVA followed by Bonferroni's, Dunnett's, or Tukey's post hoc analysis. Error bars represent the SEM. Null hypotheses were rejected at  $P > 0.05$  ( $P < 0.05$  was considered to be statistically significant).

### Supporting information

**S1 Data. Underlying numerical data and statistical analysis for figure panels Fig 1A, 1B, 1E, 1G and 1H; Fig 2B, 2C and 2E; Fig 3A, 3B, 3C, 3D, 3E and 3F; Fig 4C; Fig 5A, 5B, 5C, 5D and 5E; Fig 7A, 7B, 7C and 7D; Fig 8C, 8D, 8E and 8F; S1A, S1B and S1C Fig; S2A, S2B, S2C and S2D Fig; S3D, S3E and S3F Fig; S4B Fig; S5A and S5B Fig; S6 Fig; S8 Fig; S9A and S9B Fig; and S10A, S10B and S10C Fig.**

(XLSX)

**S1 Raw Images. Original images supporting all blot and gel results reported in Figs 1D, 5A, 5B, 5C, 5D, 5E, 6A, 6B, 6C, 7A, 7B, 7C, 7D, S3B, S7, S9A, S10C and S11.** The loading order, experimental samples, and molecular weight markers are indicated. The lanes used in the final figure are marked with a red box.

(PDF)

**S1 Table. Significantly altered components in the ubiquitin-modified proteome in WT versus CAM-USP6 mice.** CAM, CamK2a; USP, ubiquitin-specific protease; WT, wild-type.

(XLSX)

**S1 Fig. CAM-USP6 mice show no gross physiological or behavioral deficits.** (A) Body weight of 2-month-old WT and CAM-USP6 mice in line 1 (USP6 Tg#1) and line 2 (USP6

Tg#2). USP6 Tg#1 (WT:  $n = 18$  mice; CAM-USP6:  $n = 22$  mice). USP6 Tg#2 (WT:  $n = 15$  mice; CAM-USP6:  $n = 24$  mice). Data represent means  $\pm$  SEM. (B) Distance traveled in WT and CAM-USP6 mice from independent USP6 Tg#1 and USP6 Tg#2 lines in open field tests. USP6 Tg#1 (WT:  $n = 18$  mice; CAM-USP6:  $n = 22$  mice). USP6 Tg#2 (WT:  $n = 15$  mice; CAM-USP6:  $n = 24$  mice). Data represent means  $\pm$  SEM. (C) Time spent in the center area during open field tests in WT and CAM-USP6 mice. USP6 Tg#1 (WT:  $n = 18$  mice; CAM-USP6:  $n = 22$  mice). USP6 Tg#2 (WT:  $n = 15$  mice; CAM-USP6:  $n = 24$  mice). Data represent means  $\pm$  SEM. No significant difference was observed as determined by a Student  $t$  test. The underlying data for this figure can be found in [S1 Data](#). CAM, CamK2a; Tg, transgenic; USP, ubiquitin-specific protease; WT, wild-type. (EPS)

**S2 Fig. Overexpression of USP6 enhances spatial memory of CAM-USP6 mice in Morris water maze tests.** (A) Morris water maze test results as determined by escape latency to find a hidden platform. Data represent means  $\pm$  SEM. WT:  $n = 10$  mice; CAM-USP6 (line 2):  $n = 18$  mice.  $*P < 0.05$  as determined by repeated-measure ANOVA with Bonferroni's post hoc analysis. (B) Swimming speed of mice subjected to the Morris water maze test. Data represent means  $\pm$  SEM. WT:  $n = 10$  mice; CAM-USP6 (line 2):  $n = 18$  mice. No significance was observed, as determined by repeated-measures ANOVA with Bonferroni's post hoc analysis. (C) Morris water maze probe test results of WT and CAM-USP6 (line 2) mice. Data represent means  $\pm$  SEM. WT:  $n = 10$  mice; CAM-USP6 (line 2):  $n = 18$  mice.  $*P < 0.05$  determined by a Student  $t$  test. The target was situated in the SW quadrant. (D) Morris water maze probe test: percentage time spent in platform area in WT and CAM-USP6 (line 2) mice. Data represent means  $\pm$  SEM. WT:  $n = 10$  mice; CAM-USP6 (line 2):  $n = 18$  mice.  $*P < 0.05$  determined by a Student  $t$  test. The underlying data for this figure can be found in [S1 Data](#). CAM, CamK2a; SW, southwest; USP, ubiquitin-specific protease; WT, wild-type. (EPS)

**S3 Fig. Nestin-USP6 mice feature no gross anatomical abnormalities.** (A) Schematic diagram of constructs used to generate USP6 transgenic mouse lines under the regulation of a Nestin promoter (Nestin-USP6). (B) Immunoblot analysis to detect USP6-HA expression in brain from E18.5 Nestin-USP6 mouse embryos. (C) Immunostaining for BLBP in E16.5 WT and Nestin-USP6 mouse brain. Scale bar = 200  $\mu\text{m}$ . (D) Sagittal sections of P0 WT and Nestin-USP6 mouse brain were analyzed by Nissl staining. Data represent means  $\pm$  SEM.  $n = 3$  mice per genotype. No significance was observed as determined by a Student  $t$  test. Scale bar = 500  $\mu\text{m}$ . (E) Sagittal sections from P60 WT and Nestin-USP6 mouse brain were analyzed by Nissl staining. Data represent means  $\pm$  SEM.  $n = 3$  mice per genotype. Values were not statistically significant as determined by a Student  $t$  test. Scale bar = 1,000  $\mu\text{m}$ . (F) Immunostaining and quantification of CUX1<sup>+</sup> and CTIP2<sup>+</sup> in E16.5 WT and Nestin-USP6 mouse cortex. Scale bar = 100  $\mu\text{m}$ . Data represent means  $\pm$  SEM.  $n = 3$  mice per genotype. No statistically significant differences were determined by Student  $t$  test. Scale bar = 100  $\mu\text{m}$ . The underlying data for this figure can be found in [S1 Data](#). BLBP, Brain lipid-binding protein; CTIP2, COUP-TF-interacting protein 2; CUX1, cut like homeobox 1; E, embryonic day; HA, hemagglutinin; P, postnatal day; USP, ubiquitin-specific protease; WT, wild-type. (EPS)

**S4 Fig. CAM-USP6 mice feature normal brain morphology.** (A) Sagittal sections from 2-month-old WT and CAM-USP6 mouse brain were analyzed by Nissl staining. Scale bar = 1,000  $\mu\text{m}$ ; scale bar (zoom in) = 200  $\mu\text{m}$ . (B) Cortical thickness of 2-month-old WT and CAM-USP6 mice. Data represent means  $\pm$  SEM.  $n = 3$  mice per genotype. Not significant as

determined by a Student *t* test. The underlying data for this figure can be found in [S1 Data](#). CAM, CamK2a; USP, ubiquitin-specific protease; WT, wild-type. (EPS)

**S5 Fig. USP6 increases spine density in CAM-USP6 mice.** (A) TEM analysis and synapse quantification of 2-month-old WT and CAM-USP6 mouse cortex and hippocampus. Scale bar = 500 nm. Data represent means  $\pm$  SEM.  $n = 4$  mice per genotype. \*\*\*\* $P < 0.0001$  determined by a Student *t* test. (B) Golgi staining and quantification of dendritic spines in the cortex and hippocampus of 2-month-old WT and CAM-USP6 mice. Scale bar = 5  $\mu$ m. Data represent means  $\pm$  SEM.  $n = 4$  mice per genotype. \*\*\*\* $P < 0.0001$  determined by a Student *t* test. The underlying data for this figure can be found in [S1 Data](#). CAM, CamK2a; NS, not significant; TEM, transmission electron microscopy; USP, ubiquitin-specific protease; WT, wild-type. (EPS)

**S6 Fig. AMPA receptor-mediated synaptic transmission in CAM-USP6 mice.** Representative mEPSC recordings in CA1 neurons from 1-month-old WT ( $n = 4$  mice, 16 cells) and CAM-USP6 ( $n = 4$  mice, 15 cells) hippocampal slices. Data represent means  $\pm$  SEM. Not significant as determined by a Student *t* test. The underlying data for this figure can be found in [S1 Data](#). AMPA,  $\alpha$ -amino-3-hydroxy-5-methyl-4-isoxazolepropionic acid; CAM, CamK2a; mEPSC, miniature excitatory postsynaptic current; USP, ubiquitin-specific protease; WT, wild-type. (EPS)

**S7 Fig. Distribution of USP6 in biochemical synaptic fractions.** Immunoblot analysis of USP6-HA in S1 (postnucleus), synaptosomal, and PSD fractions from WT and CAM-USP6 mouse cortex. CAM, CamK2a; HA, hemagglutinin; PSD, postsynaptic density; USP, ubiquitin-specific protease; WT, wild-type. (EPS)

**S8 Fig. Glutamate receptor mRNA expression remains unchanged in CAM-USP6 mouse brains.** GluN1, GluN2A, GluN2B, GluA1, and GluA2 mRNA levels relative to  $\beta$ -actin from WT and CAM-USP6 mouse cortex were determined by qRT-PCR analysis. Data represent means  $\pm$  SEM;  $n = 3$  mice per genotype. Not significant as determined by Student *t* test. The underlying data for this figure can be found in [S1 Data](#). CAM, CamK2a; Glu, glutamate ionotropic receptor; qRT-PCR, quantitative reverse transcription PCR; USP, ubiquitin-specific protease; WT, wild-type. (EPS)

**S9 Fig. Characterizing knockdown efficiency of USP6-targeting shRNA.** (A) USP6 depletion with USP6-targeting shRNAs in USP6-Flag-transfected HEK293T cells. Signal intensities from immunoblots were normalized to  $\beta$ -actin.  $n = 3$ . \* $P < 0.05$  as determined by one-way ANOVA with Tukey's post hoc analysis. (B) Knockdown of endogenous USP6 using USP6-targeting shRNAs in HEK293T cells. USP6 mRNA expression levels were measured by qRT-PCR. Data represent means  $\pm$  SEM.  $n = 9$ . \* $P < 0.05$ , \*\* $P < 0.01$  as determined by one-way ANOVA with Tukey's post hoc analysis. The underlying data for this figure can be found in [S1 Data](#). qRT-PCR, quantitative reverse transcription PCR; shRNA, short hairpin RNA; USP, ubiquitin-specific protease. (EPS)

**S10 Fig. Depletion of TBC1D3 and USP32 did not affect GluN1 expression.** (A) Knockdown efficiency of TBC1D3 siRNA in HEK293T cells was evaluated by qRT-PCR. Data

represent means  $\pm$  SEM.  $n = 6$ .  $*P < 0.05$ ,  $****P < 0.0001$  as determined by a Student *t* test. (B) Knockdown efficiency of USP32-targeting siRNAs in HEK293T cells was evaluated by qRT-PCR. Data represent means  $\pm$  SEM.  $n = 6$ .  $*P < 0.05$ ,  $***P < 0.001$ ,  $****P < 0.0001$  determined by Student *t* test. (C) Immunoblot analysis of GluN1 levels in GluN1-expressing HEK293T cells transfected with TBC1D3/USP32 siRNAs. Signal intensities were normalized to  $\beta$ -actin.  $n = 3$ . Not significant as determined by one-way ANOVA with Tukey's post hoc analysis. The underlying data for this figure can be found in [S1 Data](#). Glu, glutamate ionotropic receptor; qRT-PCR, quantitative reverse transcription PCR; siRNA, small interfering RNA; TBC, Tre-2/USP6, BUB2, and Cdc16; TBC1D3, TBC1 domain family member 3; USP, ubiquitin-specific protease. (EPS)

**S11 Fig. USP6 reduces levels of polyubiquitin-conjugated GluN1 and GluN2B subunits in HEK293T cells.** Immunoblot analysis of polyubiquitinated GluN1 and GluN2B levels in USP6-Flag- and GluN1-Myc/GluN2B-Myc-transfected HEK293T cells. Cell lysates were immunoprecipitated with Myc-magnetic beads and immunoblotted with anti-Flag, ubiquitin, or Myc antibodies as indicated. Glu, glutamate ionotropic receptor; USP, ubiquitin-specific protease. (EPS)

## Acknowledgments

We thank Luming Yao for the specimen preparation in TEM analysis. We thank Ying Zheng for the assistance in behavioral tests, Shuo Zhang for data analysis, and Nawen Wang for the assistance in genotyping of transgenic mice. We also thank APTBIO Company for their technical assistance in proteomic analysis and Xiamen University Laboratory Animal Center for animal care.

## Author Contributions

**Conceptualization:** Xin Wang.

**Data curation:** Fanwei Zeng.

**Formal analysis:** Fanwei Zeng, Lin Zhu, Ying Zhou, Xin Wang.

**Funding acquisition:** Xin Wang.

**Investigation:** Fanwei Zeng, Xuehai Ma, Lin Zhu, Qiang Xu, Yuzhe Zeng, Yue Gao, Guilin Li, Tiantian Guo, Haibin Zhang, Xiaoyan Tang, Ziqiang Wang, Zesen Ye, Kunping Li, Jinfang Lu, Xueting Qi, Xin Wang.

**Methodology:** Fanwei Zeng, Xuehai Ma, Lin Zhu, Hongfeng Zhang, Qiuyang Zheng, Hong Luo, Xian Zhang, Zhanxiang Wang, Rongqin Ke, Ying Zhou, Yan Liu, Hao Sun, Zhicheng Shao, Xin Wang.

**Project administration:** Xin Wang.

**Resources:** Liangkai Zheng, Yulin Zhou, Yi Yao.

**Software:** Fanwei Zeng.

**Supervision:** Xin Wang.

**Visualization:** Fanwei Zeng, Xuehai Ma, Lin Zhu, Qiang Xu, Yuzhe Zeng, Haibin Zhang.

**Writing – original draft:** Fanwei Zeng, Xin Wang.

**Writing – review & editing:** Timothy Huang, Huaxi Xu, Xin Wang.

## References

- Ju XC, Hou QQ, Sheng AL, Wu KY, Zhou Y, et al. (2016) The hominoid-specific gene TBC1D3 promotes generation of basal neural progenitors and induces cortical folding in mice. *Elife* 5. pii: e18197. <https://doi.org/10.7554/eLife.18197> PMID: 27504805
- Liu J, Liu W, Yang L, Wu Q, Zhang H, et al. (2017) The Primate-Specific Gene TMEM14B Marks Outer Radial Glia Cells and Promotes Cortical Expansion and Folding. *Cell Stem Cell* 21: 635–649.e638. <https://doi.org/10.1016/j.stem.2017.08.013> PMID: 29033352
- Florio M, Albert M, Taverna E, Namba T, Brandl H, et al. (2015) Human-specific gene ARHGAP11B promotes basal progenitor amplification and neocortex expansion. *Science* 347: 1465–1470. <https://doi.org/10.1126/science.aaa1975> PMID: 25721503
- Suzuki IK, Gacquer D, Van Heurck R, Kumar D, Wojno M, et al. (2018) Human-Specific NOTCH2NL Genes Expand Cortical Neurogenesis through Delta/Notch Regulation. *Cell* 173: 1370–1384.e1316. <https://doi.org/10.1016/j.cell.2018.03.067> PMID: 29856955
- Fiddes IT, Lodewijk GA, Mooring M, Bosworth CM, Ewing AD, et al. (2018) Human-Specific NOTCH2NL Genes Affect Notch Signaling and Cortical Neurogenesis. *Cell* 173: 1356–1369.e1322. <https://doi.org/10.1016/j.cell.2018.03.051> PMID: 29856954
- Pakkenberg B, Pelvig D, Marner L, Bundgaard MJ, Gundersen HJ, et al. (2003) Aging and the human neocortex. *Exp Gerontol* 38: 95–99. [https://doi.org/10.1016/s0531-5565\(02\)00151-1](https://doi.org/10.1016/s0531-5565(02)00151-1) PMID: 12543266
- Elston GN, Benavides-Piccione R, DeFelipe J (2001) The pyramidal cell in cognition: a comparative study in human and monkey. *J Neurosci* 21: RC163. <https://doi.org/10.1523/JNEUROSCI.21-17-j0002.2001> PMID: 11511694
- Charrier C, Joshi K, Coutinho-Budd J, Kim JE, Lambert N, et al. (2012) Inhibition of SRGAP2 function by its human-specific paralogs induces neoteny during spine maturation. *Cell* 149: 923–935. <https://doi.org/10.1016/j.cell.2012.03.034> PMID: 22559944
- Sia GM, Clem RL, Hugarir RL (2013) The human language-associated gene SRPX2 regulates synapse formation and vocalization in mice. *Science* 342: 987–991. <https://doi.org/10.1126/science.1245079> PMID: 24179158
- Roll P, Rudolf G, Pereira S, Royer B, Scheffer IE, et al. (2006) SRPX2 mutations in disorders of language cortex and cognition. *Hum Mol Genet* 15: 1195–1207. <https://doi.org/10.1093/hmg/ddl035> PMID: 16497722
- van Spronsen M, Hoogenraad CC (2010) Synapse pathology in psychiatric and neurologic disease. *Curr Neurol Neurosci Rep* 10: 207–214. <https://doi.org/10.1007/s11910-010-0104-8> PMID: 20425036
- Niciu MJ, Kelmendi B, Sanacora G (2012) Overview of glutamatergic neurotransmission in the nervous system. *Pharmacol Biochem Behav* 100: 656–664. <https://doi.org/10.1016/j.pbb.2011.08.008> PMID: 21889952
- Sheng M, Kim E (2011) The postsynaptic organization of synapses. *Cold Spring Harb Perspect Biol* 3. pii: a005678. <https://doi.org/10.1101/cshperspect.a005678> PMID: 22046028
- Luscher C, Malenka RC (2012) NMDA receptor-dependent long-term potentiation and long-term depression (LTP/LTD). *Cold Spring Harb Perspect Biol* 4. pii: a005710. <https://doi.org/10.1101/cshperspect.a005710> PMID: 22510460
- Chen W, Shieh C, Swanger SA, Tankovic A, Au M, et al. (2017) GRIN1 mutation associated with intellectual disability alters NMDA receptor trafficking and function. *J Hum Genet* 62: 589–597. <https://doi.org/10.1038/jhg.2017.19> PMID: 28228639
- Hu C, Chen W, Myers SJ, Yuan H, Traynelis SF (2016) Human GRIN2B variants in neurodevelopmental disorders. *J Pharmacol Sci* 132: 115–121. <https://doi.org/10.1016/j.jphs.2016.10.002> PMID: 27818011
- Geisheker MR, Heymann G, Wang T, Coe BP, Turner TN, et al. (2017) Hotspots of missense mutation identify neurodevelopmental disorder genes and functional domains. *Nat Neurosci* 20: 1043–1051. <https://doi.org/10.1038/nn.4589> PMID: 28628100
- Ehlers MD (2003) Activity level controls postsynaptic composition and signaling via the ubiquitin-proteasome system. *Nat Neurosci* 6: 231–242. <https://doi.org/10.1038/nn1013> PMID: 12577062
- Kato A, Rouach N, Nicoll RA, Bredt DS (2005) Activity-dependent NMDA receptor degradation mediated by retrotranslocation and ubiquitination. *Proc Natl Acad Sci U S A* 102: 5600–5605. <https://doi.org/10.1073/pnas.0501769102> PMID: 15809437

20. Jurd R, Thornton C, Wang J, Luong K, Phamluong K, et al. (2008) Mind bomb-2 is an E3 ligase that ubiquitinates the N-methyl-D-aspartate receptor NR2B subunit in a phosphorylation-dependent manner. *J Biol Chem* 283: 301–310. <https://doi.org/10.1074/jbc.M705580200> PMID: 17962190
21. Lin A, Hou Q, Jarzyl L, Amato S, Gilbert J, et al. (2011) Nedd4-mediated AMPA receptor ubiquitination regulates receptor turnover and trafficking. *J Neurochem* 119: 27–39. <https://doi.org/10.1111/j.1471-4159.2011.07221.x> PMID: 21338354
22. Fu AK, Hung KW, Fu WY, Shen C, Chen Y, et al. (2011) APC(Cdh1) mediates EphA4-dependent down-regulation of AMPA receptors in homeostatic plasticity. *Nat Neurosci* 14: 181–189. <https://doi.org/10.1038/nn.2715> PMID: 21186356
23. Paulding CA, Ruvolo M, Haber DA (2003) The Tre2 (USP6) oncogene is a hominoid-specific gene. *Proc Natl Acad Sci U S A* 100: 2507–2511. <https://doi.org/10.1073/pnas.0437015100> PMID: 12604796
24. Ou Z, Jarmuz M, Sparagana SP, Michaud J, Decarie JC, et al. (2006) Evidence for involvement of TRE-2 (USP6) oncogene, low-copy repeat and acrocentric heterochromatin in two families with chromosomal translocations. *Hum Genet* 120: 227–237. <https://doi.org/10.1007/s00439-006-0200-7> PMID: 16791615
25. Tentler D, Johannesson T, Johannsson M, Rastam M, Gillberg C, et al. (2003) A candidate region for Asperger syndrome defined by two 17p breakpoints. *Eur J Hum Genet* 11: 189–195. <https://doi.org/10.1038/sj.ejhg.5200939> PMID: 12634868
26. Tsien JZ, Chen DF, Gerber D, Tom C, Mercer EH, et al. (1996) Subregion- and cell type-restricted gene knockout in mouse brain. *Cell* 87: 1317–1326. [https://doi.org/10.1016/s0092-8674\(00\)81826-7](https://doi.org/10.1016/s0092-8674(00)81826-7) PMID: 8980237
27. Fischer J, Hammerschmidt K (2011) Ultrasonic vocalizations in mouse models for speech and socio-cognitive disorders: insights into the evolution of vocal communication. *Genes Brain Behav* 10: 17–27. <https://doi.org/10.1111/j.1601-183X.2010.00610.x> PMID: 20579107
28. Crawley JN (2007) Mouse behavioral assays relevant to the symptoms of autism. *Brain Pathol* 17: 448–459. <https://doi.org/10.1111/j.1750-3639.2007.00096.x> PMID: 17919130
29. Martinez LA, Tejada-Simon MV (2011) Pharmacological inactivation of the small GTPase Rac1 impairs long-term plasticity in the mouse hippocampus. *Neuropharmacology* 61: 305–312. <https://doi.org/10.1016/j.neuropharm.2011.04.017> PMID: 21569781
30. Wu D, Bacaj T, Morishita W, Goswami D, Arendt KL, et al. (2017) Postsynaptic synaptotagmins mediate AMPA receptor exocytosis during LTP. *Nature* 544: 316–321. <https://doi.org/10.1038/nature21720> PMID: 28355182
31. Bingol B, Schuman EM (2006) Activity-dependent dynamics and sequestration of proteasomes in dendritic spines. *Nature* 441: 1144–1148. <https://doi.org/10.1038/nature04769> PMID: 16810255
32. Fonseca R, Vabulas RM, Hartl FU, Bonhoeffer T, Nagerl UV (2006) A balance of protein synthesis and proteasome-dependent degradation determines the maintenance of LTP. *Neuron* 52: 239–245. <https://doi.org/10.1016/j.neuron.2006.08.015> PMID: 17046687
33. Jiang YH, Armstrong D, Albrecht U, Atkins CM, Noebels JL, et al. (1998) Mutation of the Angelman ubiquitin ligase in mice causes increased cytoplasmic p53 and deficits of contextual learning and long-term potentiation. *Neuron* 21: 799–811. [https://doi.org/10.1016/s0896-6273\(00\)80596-6](https://doi.org/10.1016/s0896-6273(00)80596-6) PMID: 9808466
34. van Woerden GM, Harris KD, Hojjati MR, Gustin RM, Qiu S, et al. (2007) Rescue of neurological deficits in a mouse model for Angelman syndrome by reduction of alphaCaMKII inhibitory phosphorylation. *Nat Neurosci* 10: 280–282. <https://doi.org/10.1038/nn1845> PMID: 17259980
35. Yashiro K, Riday TT, Condon KH, Roberts AC, Bernardo DR, et al. (2009) Ube3a is required for experience-dependent maturation of the neocortex. *Nat Neurosci* 12: 777–783. <https://doi.org/10.1038/nn.2327> PMID: 19430469
36. Weeber EJ, Jiang YH, Elgersma Y, Varga AW, Carrasquillo Y, et al. (2003) Derangements of hippocampal calcium/calmodulin-dependent protein kinase II in a mouse model for Angelman mental retardation syndrome. *J Neurosci* 23: 2634–2644. <https://doi.org/10.1523/JNEUROSCI.23-07-02634.2003> PMID: 12684449
37. Ing B, Shteiman-Kotler A, Castelli M, Henry P, Pak Y, et al. (2007) Regulation of Commissureless by the ubiquitin ligase Dnedd4 is required for neuromuscular synaptogenesis in *Drosophila melanogaster*. *Mol Cell Biol* 27: 481–496. <https://doi.org/10.1128/MCB.00463-06> PMID: 17074801
38. Scudder SL, Goo MS, Cartier AE, Molteni A, Schwarz LA, et al. (2014) Synaptic strength is bidirectionally controlled by opposing activity-dependent regulation of Nedd4-1 and USP8. *J Neurosci* 34: 16637–16649. <https://doi.org/10.1523/JNEUROSCI.2452-14.2014> PMID: 25505317
39. Li M, Shin YH, Hou L, Huang X, Wei Z, et al. (2008) The adaptor protein of the anaphase promoting complex Cdh1 is essential in maintaining replicative lifespan and in learning and memory. *Nat Cell Biol* 10: 1083–1089. <https://doi.org/10.1038/ncb1768> PMID: 19160489

40. Pick JE, Malumbres M, Klann E (2012) The E3 ligase APC/C-Cdh1 is required for associative fear memory and long-term potentiation in the amygdala of adult mice. *Learn Mem* 20: 11–20. <https://doi.org/10.1101/lm.027383.112> PMID: 23242419
41. Collingridge GL, Isaac JT, Wang YT (2004) Receptor trafficking and synaptic plasticity. *Nat Rev Neurosci* 5: 952–962. <https://doi.org/10.1038/nrn1556> PMID: 15550950
42. Liu L, Wong TP, Pozza MF, Lingenhoehl K, Wang Y, et al. (2004) Role of NMDA receptor subtypes in governing the direction of hippocampal synaptic plasticity. *Science* 304: 1021–1024. <https://doi.org/10.1126/science.1096615> PMID: 15143284
43. Zheng Q, Huang T, Zhang L, Zhou Y, Luo H, et al. (2016) Dysregulation of Ubiquitin-Proteasome System in Neurodegenerative Diseases. *Front Aging Neurosci* 8: 303. <https://doi.org/10.3389/fnagi.2016.00303> PMID: 28018215
44. Ciechanover A, Brundin P (2003) The ubiquitin proteasome system in neurodegenerative diseases: sometimes the chicken, sometimes the egg. *Neuron* 40: 427–446. [https://doi.org/10.1016/s0896-6273\(03\)00606-8](https://doi.org/10.1016/s0896-6273(03)00606-8) PMID: 14556719
45. Xu H, Sweeney D, Wang R, Thinakaran G, Lo AC, et al. (1997) Generation of Alzheimer beta-amyloid protein in the trans-Golgi network in the apparent absence of vesicle formation. *Proc Natl Acad Sci U S A* 94: 3748–3752. <https://doi.org/10.1073/pnas.94.8.3748> PMID: 9108049
46. Zhong L, Wang Z, Wang D, Wang Z, Martens YA, et al. (2018) Amyloid-beta modulates microglial responses by binding to the triggering receptor expressed on myeloid cells 2 (TREM2). *Mol Neurodegener* 13: 15. <https://doi.org/10.1186/s13024-018-0247-7> PMID: 29587871
47. Pasca AM, Sloan SA, Clarke LE, Tian Y, Makinson CD, et al. (2015) Functional cortical neurons and astrocytes from human pluripotent stem cells in 3D culture. *Nat Methods* 12: 671–678. <https://doi.org/10.1038/nmeth.3415> PMID: 26005811
48. Shao Z, Noh H, Bin Kim W, Ni P, Nguyen C, et al. (2019) Dysregulated protocadherin-pathway activity as an intrinsic defect in induced pluripotent stem cell-derived cortical interneurons from subjects with schizophrenia. *Nat Neurosci* 22: 229–242. <https://doi.org/10.1038/s41593-018-0313-z> PMID: 30664768
49. Wang R, Tang Y, Feng B, Ye C, Fang L, et al. (2007) Changes in hippocampal synapses and learning-memory abilities in age-increasing rats and effects of tetrahydroxystilbene glucoside in aged rats. *Neuroscience* 149: 739–746. <https://doi.org/10.1016/j.neuroscience.2007.07.065> PMID: 17935895
50. Wang X, Zhao Y, Zhang X, Badie H, Zhou Y, et al. (2013) Loss of sorting nexin 27 contributes to excitatory synaptic dysfunction by modulating glutamate receptor recycling in Down's syndrome. *Nat Med* 19: 473–480. <https://doi.org/10.1038/nm.3117> PMID: 23524343
51. Qiu Z, Ghosh A (2008) A calcium-dependent switch in a CREST-BRG1 complex regulates activity-dependent gene expression. *Neuron* 60: 775–787. <https://doi.org/10.1016/j.neuron.2008.09.040> PMID: 19081374
52. Xie X, Kang H, Liu W, Wang GL (2015) Comprehensive profiling of the rice ubiquitome reveals the significance of lysine ubiquitination in young leaves. *J Proteome Res* 14: 2017–2025. <https://doi.org/10.1021/pr5009724> PMID: 25751157
53. Li XM, Chao DY, Wu Y, Huang X, Chen K, et al. (2015) Natural alleles of a proteasome alpha2 subunit gene contribute to thermotolerance and adaptation of African rice. *Nat Genet* 47: 827–833. <https://doi.org/10.1038/ng.3305> PMID: 25985140
54. Yu J, Lai C, Shim H, Xie C, Sun L, et al. (2018) Genetic ablation of dynactin p150(Glued) in postnatal neurons causes preferential degeneration of spinal motor neurons in aged mice. *Mol Neurodegener* 13: 10. <https://doi.org/10.1186/s13024-018-0242-z> PMID: 29490687
55. Seo J, Giusti-Rodriguez P, Zhou Y, Rudenko A, Cho S, et al. (2014) Activity-dependent p25 generation regulates synaptic plasticity and Abeta-induced cognitive impairment. *Cell* 157: 486–498. <https://doi.org/10.1016/j.cell.2014.01.065> PMID: 24725413
56. Hausrat TJ, Muhia M, Gerrow K, Thomas P, Hirdes W, et al. (2015) Radixin regulates synaptic GABAA receptor density and is essential for reversal learning and short-term memory. *Nat Commun* 6: 6872. <https://doi.org/10.1038/ncomms7872> PMID: 25891999
57. Saab BJ, Georgiou J, Nath A, Lee FJ, Wang M, et al. (2009) NCS-1 in the dentate gyrus promotes exploration, synaptic plasticity, and rapid acquisition of spatial memory. *Neuron* 63: 643–656. <https://doi.org/10.1016/j.neuron.2009.08.014> PMID: 19755107
58. Nadler JJ, Moy SS, Dold G, Trang D, Simmons N, et al. (2004) Automated apparatus for quantitation of social approach behaviors in mice. *Genes Brain Behav* 3: 303–314. <https://doi.org/10.1111/j.1601-183X.2004.00071.x> PMID: 15344923